In presenting the dissertation as a partial fulfillment of the requirements for an advanced degree from the Georgia Institute of Technology, I agree that the Library of the Institute shall make it available for inspection and circulation in accordance with its regulations governing materials of this type. I agree that permission to copy from, or to publish from, this dissertation may be granted by the professor under whose direction it was written, or, in his absence, by the Dean of the Graduate Division when such copying or publication is solely for scholarly purposes and does not involve potential financial gain. It is understood that any copying from, or publication of, this dissertation which involves potential financial gain will not be allowed without written permission.

_____

_____

7/25/68

DIFFUSION OF AEROSOLS AT VARIOUS TEMPERATURES

A THESIS

Presented to

The Faculty of the Division of Graduate

Studies and Research

by

Carl W. Sandlin

In Partial Fulfillment

of the Requirements for the Degree

Master of Science in Chemical Engineering

Georgia Institute of Technology

October, 1972

DIFFUSION OF AEROSOLS AT VARIOUS TEMPERATURES

Approved: [redacted]

[redacted]
Chairman

[redacted]

[redacted]

Date approved by Chairman: 10/23/72

ACKNOWLEDGMENTS

The author is very grateful to Dr. Michael J. Matteson whose invaluable guidance and advice contributed greatly to the successful completion of this work. He is also grateful to Dr. Clyde Orr, Jr. and Dr. Jude T. Sommerfeld for having taken time to review this work. The author wishes to express thanks to Mrs. Joyce Williams and Mrs. Nancy Price for their assistance in typing.

A special thanks is included to Dr. Othmar Preining whose energy and ideas were most helpful during the early part of the work.

This work was supported in part by an Environmental Protection Agency Training Grant AP-00086-02.

TABLE OF CONTENTS

	Page
ACKNOWLEDGMENTS	ii
LIST OF TABLES	iv
LIST OF FIGURES	vi
NOMENCLATURE	viii
SUMMARY	ix
Chapter	
I. INTRODUCTION	1
II. EQUIPMENT AND INSTRUMENTATION	7
III. PROCEDURE	15
IV. PRESENTATION OF RESULTS	21
V. DISCUSSION OF RESULTS	30
VI. CONCLUSIONS	38
VII. RECOMMENDATIONS	39
APPENDIX	
A. CHS ON DIFFUSION BATTERY DATA	41
B. THEORETICAL DIFFUSION COEFFICIENT	49
C. THEORETICAL CALCULATIONS	52
D. CALCULATED DATA	56
E. EXPERIMENTAL DATA - FIRST ARRANGEMENT	62
F. EXPERIMENTAL DATA - SECOND ARRANGEMENT	77
BIBLIOGRAPHY	99

LIST OF TABLES

Table		Page
1.	CHS Dimensions	30
2.	Effect of Time on NaCl Particle Size	32
3.	Impaction Efficiency - A Function of Temperature and Particle Size	34
4.	Experimental Diffusion Coefficient	35
5.	Size Analyzer Data	41
6.	Conversion of Size Analyzer Data Considering Magnification	43
7.	Velocity of Aerosol Through CHS	45
8.	Reynold's Number Calculation	46
9.	Pressure Drop Through Diffusion Battery	47
10.	D_{Th} at 295° K	49
11.	D_{Th} at 257° K	50
12.	D_{Th} at 201° K	50
13.	Theoretical Penetration for a Given Particle Size	52
14.	Calculation of Impaction Efficiency	54
15.	Corrected N/N_o and Associated Δ	59
16.	Comparison of Theoretical and Experimental D	60
17.	Concentration Data I	62
18.	Concentration Data II	64
19.	Concentration Data III	66
20.	Concentration Data IV	68
21.	Concentration Data V	70

List of Tables (Continued)

Table		Page
22.	Concentration Data VI	72
23.	Concentration Data VII	75
24.	Concentration Data from Test 10 at 22°C	77
25.	Concentration Data from Test 15 at 22°C	80
26.	Concentration Data from Test 10 at 22°C	82
27.	Concentration Data from Test 17 at 22°C	84
28.	Concentration Data from Test 10 at -16°C	87
29.	Concentration Data from Test 16 at -16°C	89
30.	Concentration Data from Test 10 at -72°C	91
31.	Concentration Data from Test 15 at -72°C	94
32.	Concentration Data from Test 16 at -72°C	97

LIST OF FIGURES

Figure		Page
1.	Theoretical Penetration as a Function of Δ	4
2.	Theoretical Penetration as a Function of Tube Length and Particle Size	5
3.	Diffusion Battery	8
4.	Collimated Hole Structures Nominal Diameter 125 Micrometer	9
5.	Collimated Hole Structures Nominal Diameter 12.5 Micrometer	9
6.	Typical NaCl Aerosol Particles	11
7.	Experimental Apparatus	12
8.	Graphical Comparison of Theoretical and Experimental Penetration	19
9.	Sample Concentration Data: Two 125 Micrometer and Two 12.5 Micrometer Diameter CHS	22
10.	Concentration Changes of NaCl Aerosol Four CHS: Two of 125 Micrometer and Two 12.5 Micrometer Diameter	23
11.	Penetration of NaCl Aerosol: Two 125 Micrometer and Two 12.5 Micrometer Diameter CHS in Series	24
12.	Concentration Change of NaCl Aerosol Passing through Four 12.5 Micrometer Diameter CHS	26
13.	Penetration of NaCl Aerosol: Four 12.5 Micrometer Diameter CHS in Series, T = 295^{o}K	27
14.	Penetration of NaCl Aerosol: Four 12.5 Micrometer Diameter CHS in Series, T = 257^{o}K.	28
15.	Penetration of NaCl Aerosol: Four 12.5 Micrometer Diameter CHS in Series, T = 201^{o}K.	29
16.	Pressure Drop through Diffusion Battery	48

List of Figures (continued)

Figure		Page
17.	Theoretical Diffusion Coefficient	51
18.	Concentration Data I	63
19.	Concentration Data II	65
20.	Concentration Data III	67
21.	Concentration Data IV	69
22.	Concentration Data V	71
23.	Concentration Data VI	74
24.	Concentration Data VII	76
25.	Concentration Data from Test 10 at 22°C	79
26.	Concentration Data from Test 15 at 22°C	81
27.	Concentration Data from Test 16 at 22°C	83
28.	Concentration Data from Test 17 at 22°C	86
29.	Concentration Data from Test 10 at -16°C	88
30.	Concentration Data from Test 16 at -16°C	90
31.	Concentration Data from Test 10 at -72°C	93
32.	Concentration Data from Test 15 at -72°C	96
33.	Concentration Data from Test 16 at -72°C	98

NOMENCLATURE

A	Empirical constant
B	Mobility of Particles, sec/gm
b	Empirical constant
c	Mass concentration, $\mu gm/m^3$
D	Diffusion coefficient, cm^2/sec; D_{ex}, experimental; D_i, at each plate; D_{Th}, theoretical
d	Particle diameter, μm; d_{ae}, aerodynamic diameter; d_{op}, optical diameter
E	Total efficiency of particle removal by filter
F	Penetration
F_m	Force causing particle motion, gm · cm/sec^2
f	Frequency, Hz; Δf, frequency change
k	Boltzman's Constant
ℓ	Mean free path of gas molecules, cm
M	Mass concentration of aerosol, $\mu gm/m^3$
N	Number concentration of aerosol, $particles/m^3$
Q	Empirical constant
R	Tube radius, cm
r	Particle radius, cm
T	Temperature, ^oK
t	Time, sec; Δt, change in time
$\bar{u}$	Average velocity through tubes, cm/sec
V	Velocity of particles, cm/sec

x	Tube length, cm
$\bar{x}$	Mean displacement of aerosol particles due to Brownian motion, cm
Δ	Dimensionless ratio
ϵ_D	Diffusion efficiency of filter
ϵ_i	Impaction efficiency of filter
η	Viscosity of gas, gm/cm · sec
ρ	Particle density, gm/cm^3

SUMMARY

The diffusion properties of aerosols as predicted by Gormley and Kennedy have previously been experimentally verified at room temperature (27°C) using large diffusion batteries of either parallel plates or long circular tubes. It was desired in this study to test the diffusion of aerosols at low temperatures where classical Brownian motion theory may not apply. Tests were performed using a more compact diffusion battery consisting of newly developed collimated hole structures with pores of approximately 12.5 micrometers and a length to diameter ratio of 40. By measuring the aerosol mass concentration before and after flow through these holes, it has been possible to determine experimentally the diffusion coefficient and to correlate this with the theoretically predicted value. The compactness of the battery allowed it to be submerged in a low-temperature bath and the diffusion of aerosols to be tested at low temperatures.

Diffusion measurements were made at three temperatures: room temperature (22°C), H_2O(s)-acetone bath (-16°C), and CO_2(s)-acetone bath (-72°C). At all temperatures, correction was made for the extra loss of particles from the aerosol due to impaction on the face of the collimated hole structures. At room temperature, the diffusion observed experimentally correlated quite well with the theoretically predicted diffusion. However, at -16°C, the observed diffusion rate was 30-40 percent above the theoretically predicted diffusion rate. At -72°C, the difference was even more pronounced. At this lowest temperature, 50-65

percent more particle loss by diffusion than theoretically predicted was observed. Calculations showed that the value of the diffusion coefficient had been raised 2-4 times above the expected value. It was concluded that diffusion theory, which had been developed using an ideal gas assumption, does not apply at low temperatures where the gas is not ideal.

CHAPTER I

INTRODUCTION

Very small aerosol particles are characterized by relatively high diffusion rates. It is possible to use this property for measurement of particle size.

Gravity has a negligible effect on particles having a radius of 0.3 micrometer and lower in a moving gas stream. As the aerosol moves in laminar flow through a narrow channel, the random Brownian movement displaces the particles from their original position in the air flow streamlines. The most probable displacement is zero, but the mean square displacement of a particle is proportional to the travel time (1). As a result, some of the particles are displaced sufficiently to reach the walls of the channel. Since the particles have volume, i.e., cannot be considered a mathematical point, a portion of them contact the channel wall when they approach it. The attractive force between small particles and a clean surface is quite large, therefore it is quite reasonable to assume that all particles which contact the channel walls stick. Diffusion then occurs according to the following mechanism: as the aerosol travels through the channel in streamline flow, the particles near the wall are removed from the air stream. This sets up a concentration gradient in the cross section of the channel, and the particles then move, by diffusion, in the direction of decreasing concentration, i.e., toward the wall (2). A fraction, F, of the entering particles will still appear in the channel effluent. Since the magnitude of the Brownian

movement increases with decreasing particle size, the smaller the particle, the lower the value of F. The diffusion constant D of the aerosol may be obtained and the particle size determined from the value of F.

Rodebush (2) first used the term "diffusion battery"; his apparatus consisted of 40 parallel rectangular plates somewhat resembling the plates of an automobile battery. Nolan and Guerrina (3) were the first to use a diffusion battery for determining particle size. Using parallel wall channels, they found the size of atmospheric condensation nuclei. Thomas (1) used a diffusion battery consisting of 20 narrow channels from which many of the problems of the parallel plane wall diffusion battery became evident. The walls had to be very accurately machined ($\pm$ 0.00015 inch in thickness over 125 square inches); the plates had to be spaced exactly (average deviation 0.00015 inch); and an entrance port had to be provided.

Townsend (4) used channels of circular cross section; the channels were metal tubes, once again quite accurately machined. The equation developed by Townsend to describe F (penetration) was rederived in 1948 by Gormley and Kennedy (5) in the following term:

$$F = N/N_o = 0.819 \exp^{(-3.657\Delta)} + 0.097 \exp^{(-22.3\Delta)} + 0.032 \exp^{(-57\Delta)} + \ldots \quad (1)$$

where Δ is the dimensionless group:

$$\Delta = Dx/_R{}^2\overline{u} \quad (2)$$

For unsteady state conditions with small Δ, Gormley and Kennedy

gave the more accurate expression

$$N/N_o = 1 - 2.56\Delta^{2/3} + 1.2\Delta + 0.177\Delta^{4/3} \quad (3)$$

Breslin, et al., (6) in an effort to construct a rugged portable diffusion battery, used small bore tubes sealed in a single outside tube. Their most efficient battery consisted of 3000 tubes 0.073 centimeters in diameter and 60.9 centimeters in length.

The present study employed newly developed collimated hole structures in the construction of an even more compact and inexpensive diffusion battery. The collimated holes are nominally 12.5 micrometers in diameter and have an L/D ratio of 40. When placed in series, these hole structures give a unique opportunity to follow deposition (and hence diffusion) as a function of length. From the graph of Equation 3 (Figure 1), it can be seen that the larger the value of Δ, the smaller the value N/N_o (greater deposition). From Equation (2), it can be seen that the larger the value of x (length of tube), the larger the value of Δ. Therefore, for a given particle size, the theoretical deposition of particles (N/N_o) as a function of tube length can be calculated (Figure 2).

The thermal motion of particles suspended in a fluid is expressed by the following equations derived by Einstein (7).

$$\overline{x}^2 = 2Dt \quad (4)$$

$$D = kTB \quad (5)$$

The mobility, B, of a particle is the ratio of the velocity of a particle, V, to the force, F_m, causing the steady motion and may be expressed using Stokes formula as follows:

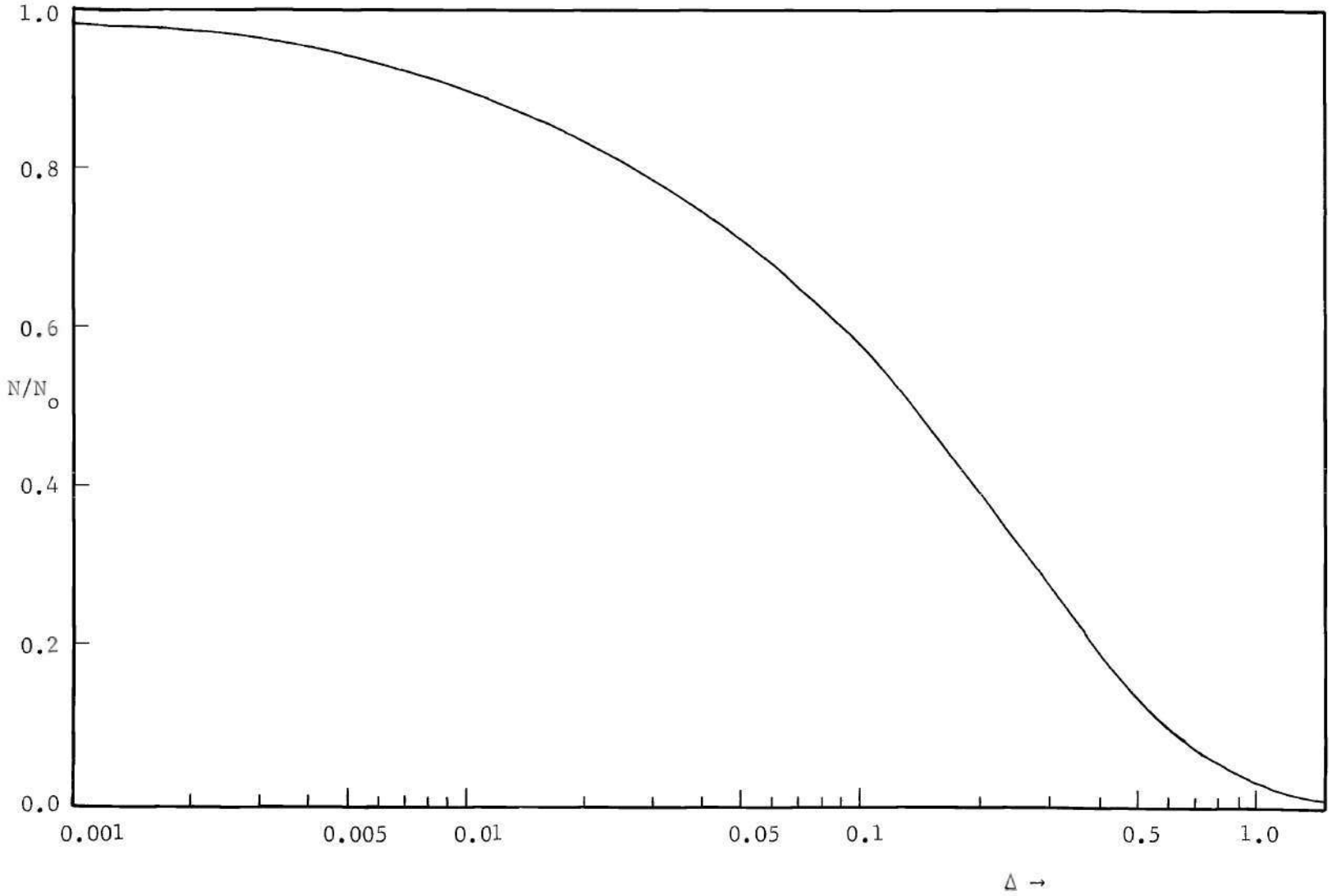

Figure 1. Theoretical Penetration as a Function of Δ

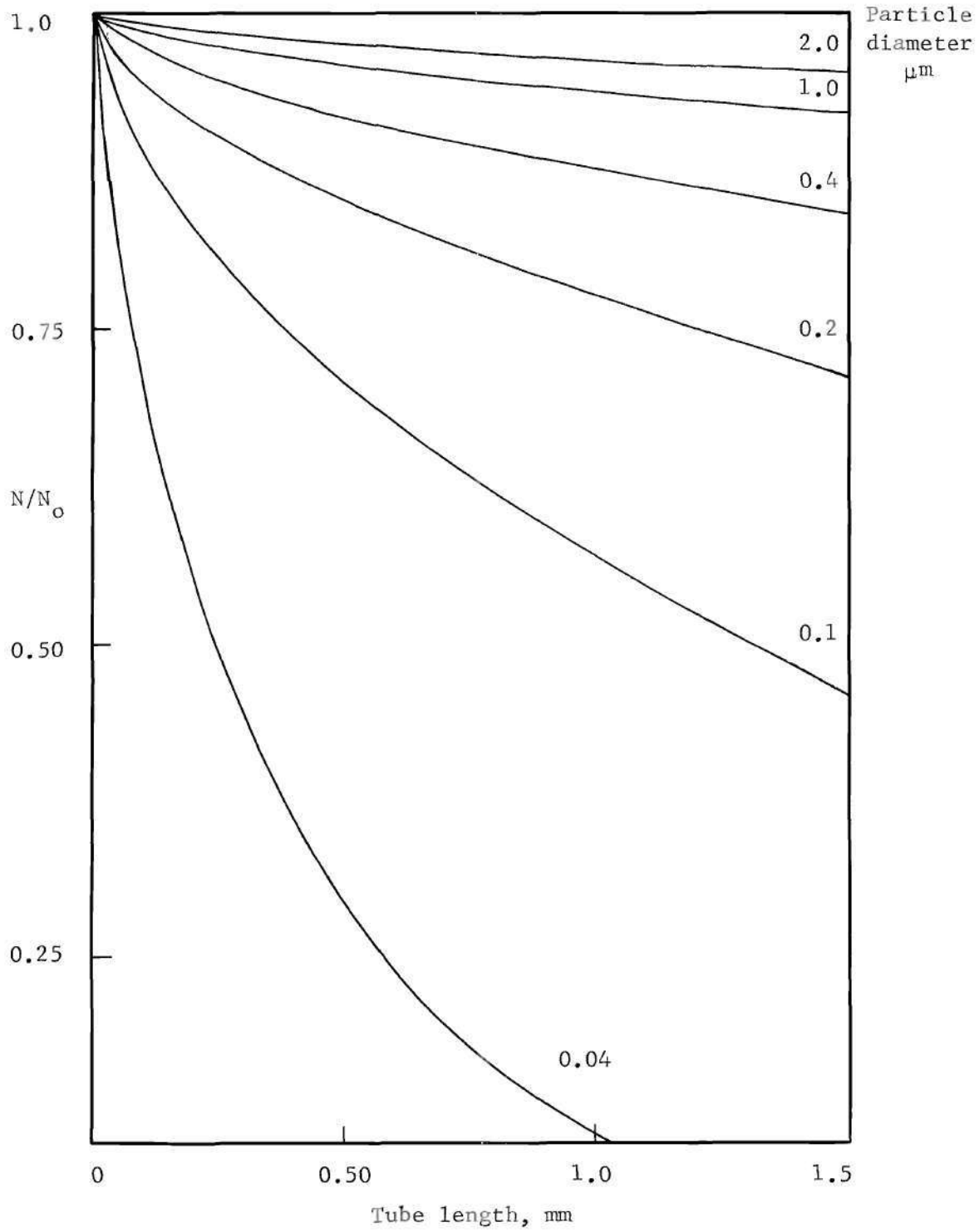

Figure 2. Theoretical Penetration as a Function of Tube Length and Particle Diameter

$$B = \frac{V}{F_m} = \frac{V}{6\pi\eta r V} = \frac{1}{6\pi\eta r} \tag{6}$$

A more accurate expression for aerosol particles (8) is

$$B = (1 + A\frac{\ell}{r} + Q\frac{\ell}{r}\exp^{-br/\ell})/6\pi\eta r \tag{7}$$

where A, Q, and b are empirical constants and ℓ is the mean free path of gas molecules. The coefficients A, Q, and b have values of 1.246, 0.42, and 0.87, respectively. The numerator of Equation (7) is a correction factor to account for the slip along the particle surface that may develop as the particle radius approaches the same order of magnitude as the mean free path of the gas molecules.

Substitution into Equation 5 shows the diffusion coefficient to be

$$D = \frac{kT}{6\pi\eta r}(1 + A\frac{\ell}{r} + Q\frac{\ell}{r}\exp^{-br/\ell}) \tag{8}$$

The diffusion coefficient is shown to be independent of particle mass but dependent on particle size and the absolute temperature of the system.

All diffusion theory has been derived using the assumption that the gas in the system will follow the Ideal Gas Law. At room temperature, this is a good assumption. However, at very low temperatures, this may not be the case. The compact size of the diffusion battery of this investigation has made it possible to submerge the battery in a low temperature bath, allowing an experimental test of the diffusion theory. Thus, the diffusion coefficient dependence on temperature can be measured.

CHAPTER II

EQUIPMENT AND INSTRUMENTATION

The main unit of the experimental apparatus is the compact diffusion battery. Newly developed collimated hole structures (CHS), made of 304 type Stainless Steel and supplied by the Brunswick Corporation Chicago, Illinois, made the compact diffusion battery possible. CHS of two sizes were acquired for the study; one set with a nominal hole diameter of 12.5 micrometer and one set with a diameter of 125 micrometer. The CHS were mounted on brass collars, Figure 3, using an epoxy resin. The plates were notched for easy identification; 1 and 2 being the nominal 125 micrometer CHS; 3, 4, 5, and 6 being the nominal 12.5 micrometer CHS. The plates were photographed with an electron microscope in order to check both the hole size and the hole size distribution, Figures 4 and 5 being representative. Positive prints were analyzed using a Zeiss Model, TGZ 3, Particle Size Analyzer. The results are shown in Appendix A.

The diffusion plates were arranged as a battery as shown in Figure 3. The diffusion battery was constructed from a section of 1-3/16 inch yellow brass. Five sampling sections, an entrance port, and an exit port were provided. The entrance port delivered the aerosol through a 1/4 inch ID tube into a 3/4 inch ID chamber. The exit port reversed the procedure; the 3/4 inch chamber was reduced to a 1/4 inch ID exit tube. The sampling sections were 1 inch lengths of the brass rod with a 3/4 inch bore. Each sampling section had a sampling port of 3/16 inch

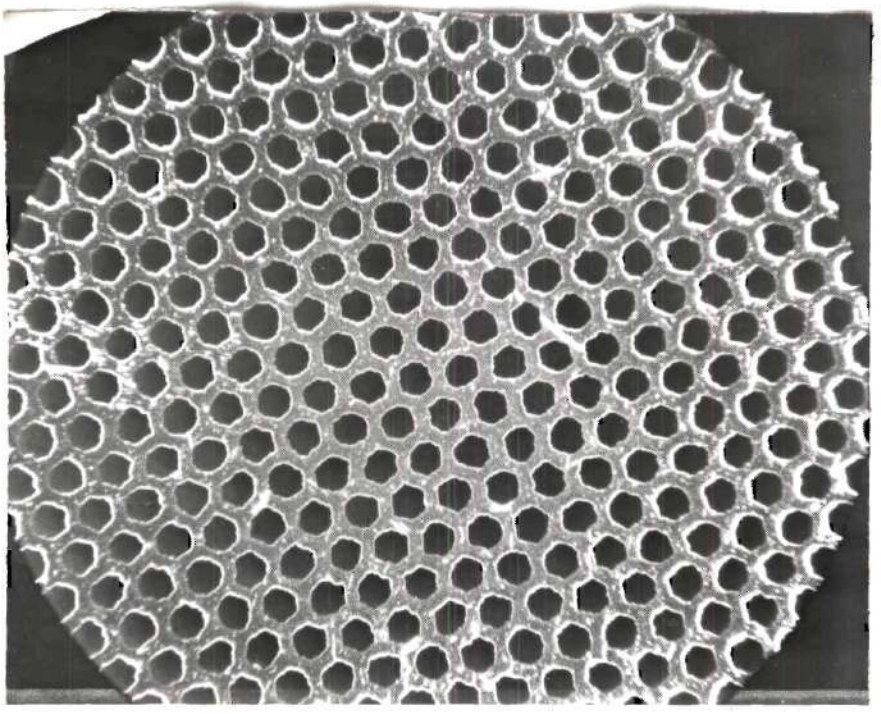

Magnification 32x

Figure 4. Collimated Hole Structures Nominal Diameter 125 μm

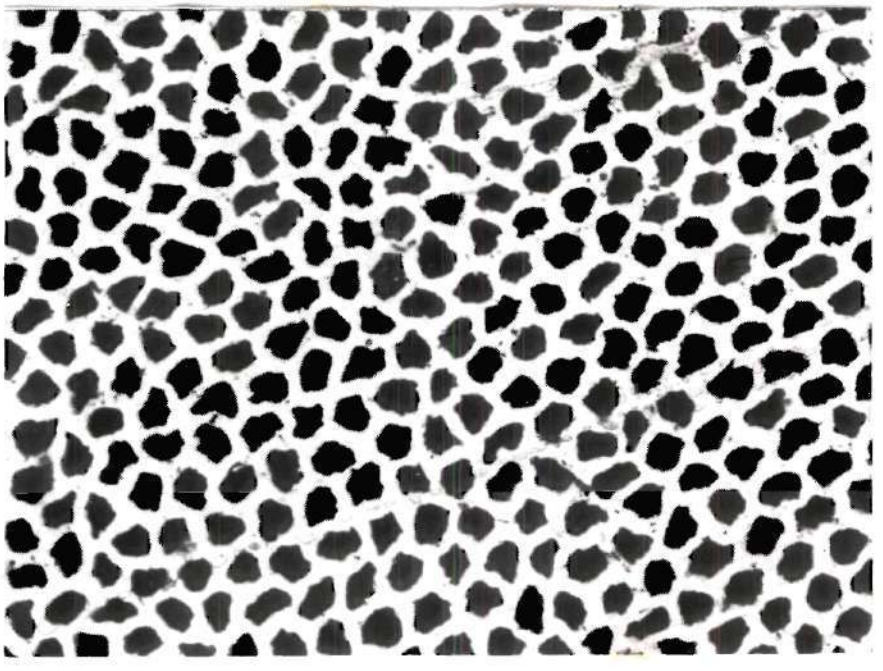

Magnification 280x

Figure 5. Collimated Hole Structures Nominal Diameter 12.5 μm

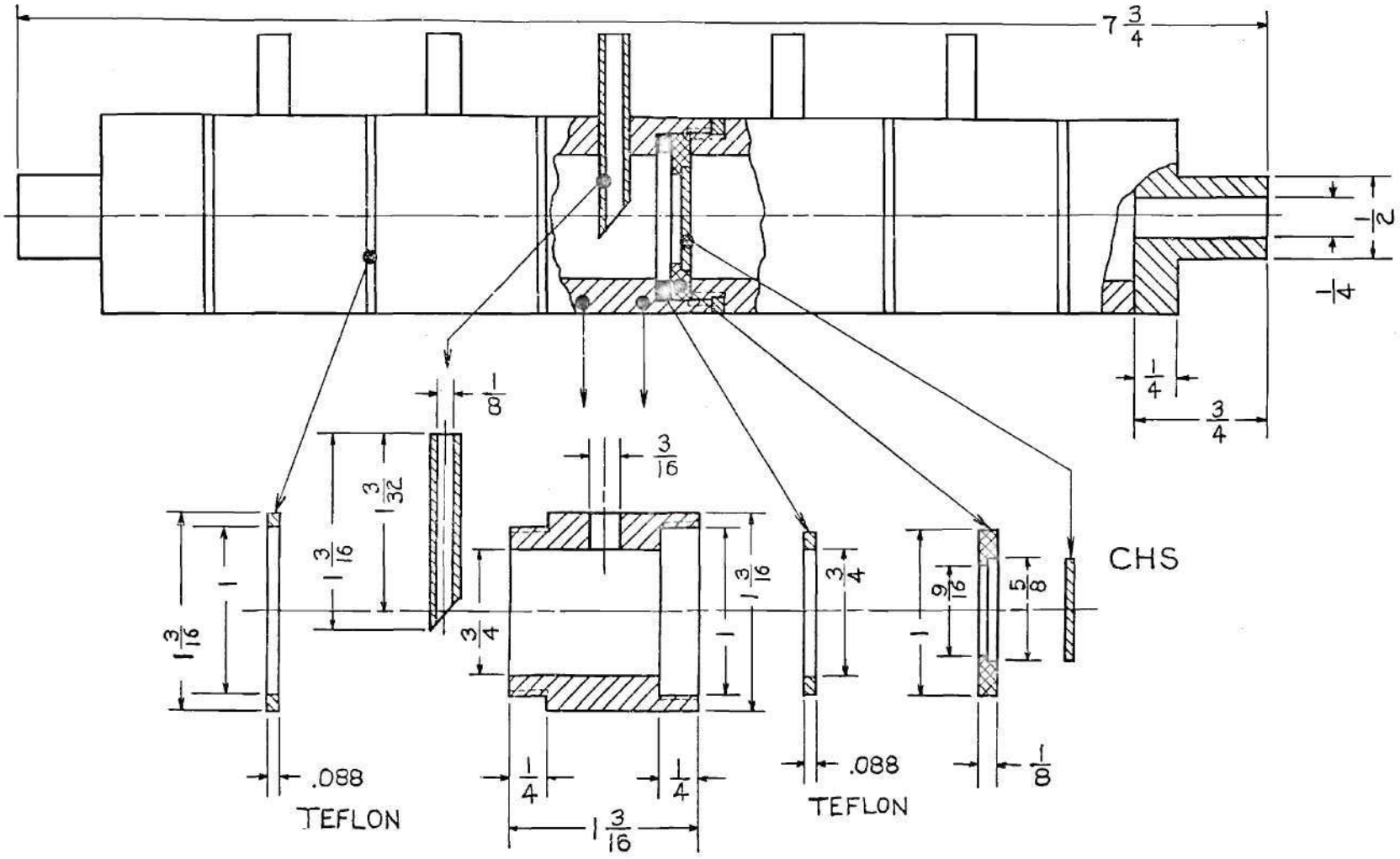

FULL SCALE
ALL DIMENSIONS IN INCHES

Figure 3. Diffusion Battery

OD by 1/8 inch ID. One diffusion plate was placed between two sampling sections; a Teflon washer on each side of the diffusion plate insured a good seal. Identical threads (12 threads per inch) in each section allowed for easy assembly and disassembly. Teflon tape was applied externally to seal the diffusion battery and to insure that no leaks were present.

The aerosol of this study contained sodium chloride particles produced by a LaMer-type aerosol generator as described by Fox (9). The generator produced monodispersed aerosol particles in the diameter range of interest in this study, 0.1 to 0.4 micrometer diameter, as shown by Figure 6. Sodium chloride was chosen because a monodispersed aerosol is easily produced from the dry solid. A further advantage of the NaCl over another aerosol, e.g., polystyrene latex, is that it allows the CHS to be easily cleaned for reuse. By immersing the CHS in distilled water and then placing the beaker in a Narda, Model G-401, ultrasonic cleaner, the plates were ready for reuse in a relatively short time.

The aerosol shown in Figure 6 is a typical sample. The aerosol, checked periodically throughout the experimental work proved consistently to be of this size uniformity. The mean particle size varied from one test to the next, but the standard deviation for a given aerosol was always near 20 percent.

The diffusion battery was then connected to sampling equipment in the experiment apparatus as shown in Figure 7. Tygon tubing (1/8 inch ID) was used to connect all the equipment.

A cold trap and a calcium chloride drying tube insured that dry air entered the dilution chamber. Wet air would allow the NaCl aerosol

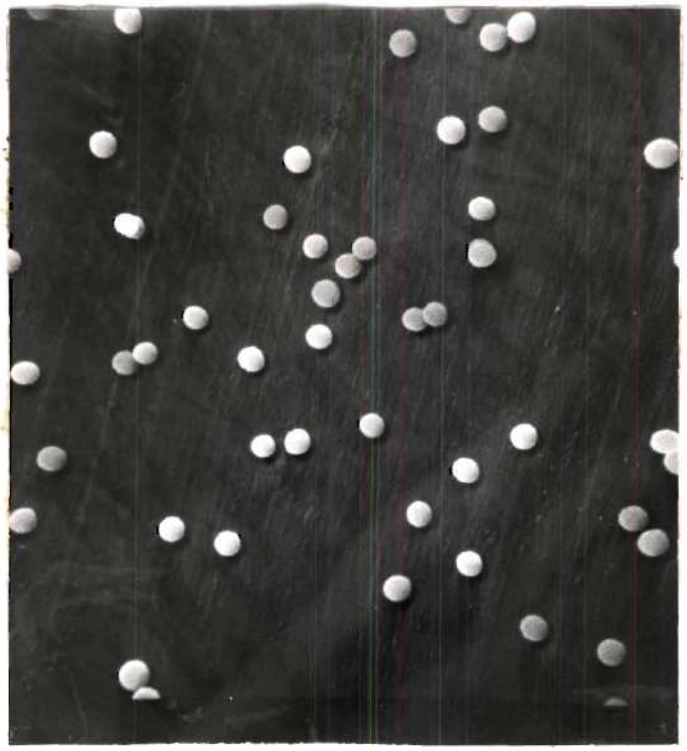

Magnification 1785x

Mean Diameter – 2.06 μm

Figure 6. Typical NaCl Aerosol Particles

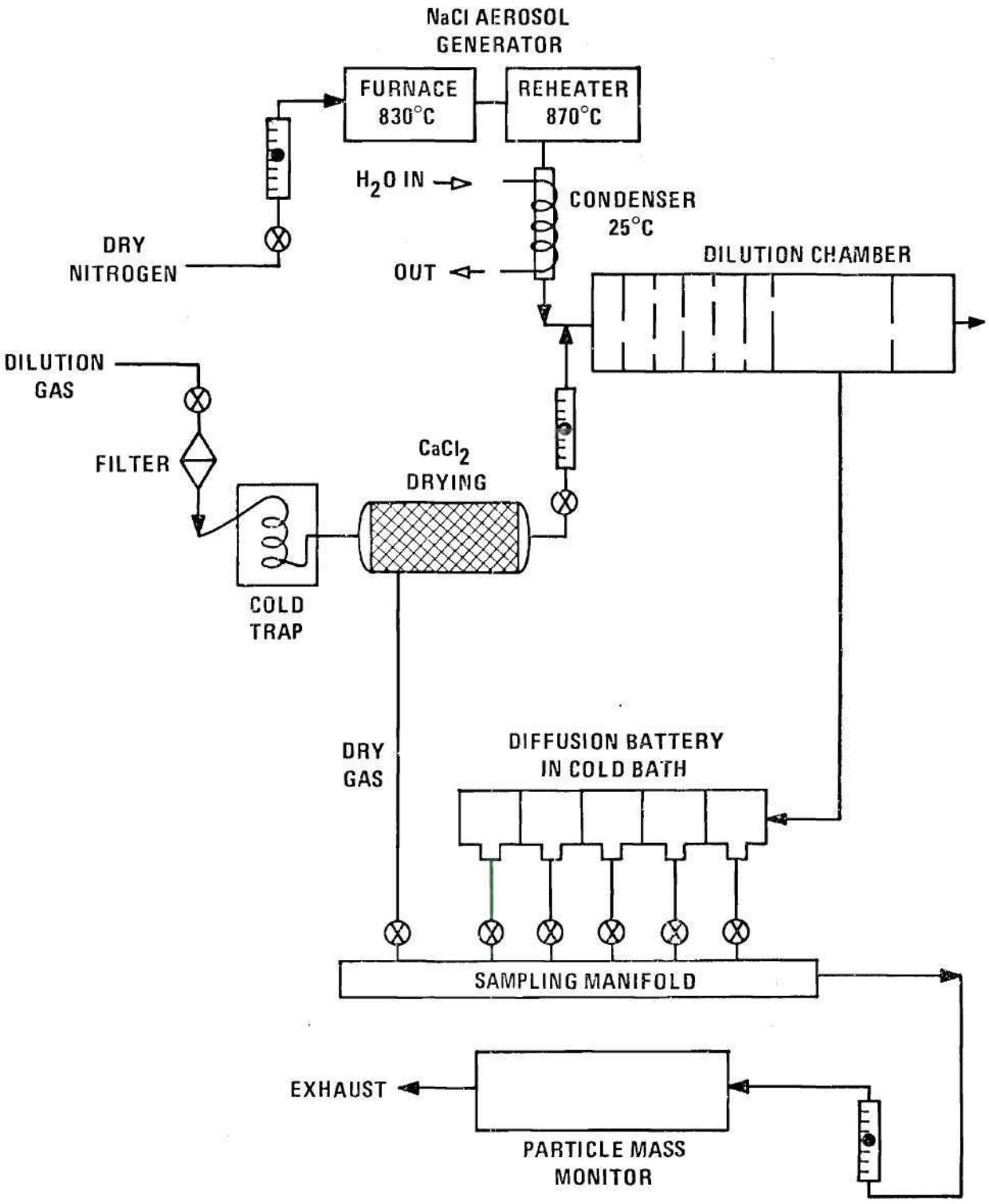

Figure 7. Experimental Apparatus

to crystalize and lose its spherical form. Also unless dry air were used, ice would form at the low temperatures and clog the system.

For the diffusion measurements at temperatures other than that of the room, an insulated Pyrex jar held the cold bath being used. A section of 1/8 inch ID copper tubing one foot in length was placed before the diffusion battery. The high thermal conductivity of the copper allowed the aerosol to cool very quickly. Temperature measurements were made using a Chromel-Alumel thermocouple and a Honeywell, Model 333, VOM Meter. They showed that the aerosol could be assumed to enter the diffusion battery at a temperature equal to the bath temperature.

A particle mass monitor, Thermo-Systems, Model 3205A, was used to follow the change in concentration of the aerosol as it passed through the diffusion battery. The particle mass monitor utilized the piezoelectric effect to measure increased mass. The resonant frequency of an oscillating quartz crystal will shift linearly downward with the added mass of particulate disposition. Two 5 MHZ, type AT, quartz crystals are employed in the mass monitor. An electrostatic precipitator charges the particles to ensure deposition on the primary crystal. The collection efficiency of the system for particles $\leq$20 micrometer diameter is stated to be 100 percent. The carrier gas continues through the system passing over the reference crystal thus compensating for changes in ambient temperature or gas adsorption. Each crystal is excited by an electronic circuit. The Thermo-Systems, Model 3202, Digital Indicator monitors and counts the frequency of a mixer circuit, giving a digital printout.

With an aerosol sampling flow rate of 1.0 liter per minute, the following equation is recommended by Thermo-Systems to obtain the

the particle mass concentration (10):

$$c = 333\ \Delta f/\Delta t, \tag{9}$$

where c is the concentration in $\mu gm/m^3$, Δf, the frequency change, is in Hz and Δt, the time, is in seconds. The concentration may be calculated from Equation (9) by dividing the total frequency shift by the time period.

The particle mass monitor measures the mass concentration of the aerosol. Diffusion theory relates penetration to the number concentration of the aerosol. The mass concentration, M, may be used in place of the number concentration, N, if the aerosol is monodisperse. For an aerosol produced by a LaMer generator, this required assumption is valid. Therefore, N has been used in place of M in the remainder of this work.

CHAPTER III

PROCEDURE

Aerosol Production

Temperature control was extremely important in the LaMer-type generator, since it was necessary to work with aerosols having a uniform size distribution. The two heaters were set at the desired temperatures (830 and 870°C, respectively) and allowed to operate continually. Reagent grade NaCl was placed in a porcelain boat and this was placed in the first heater. Dry nitrogen monitored through Matheson, R-6-15 Series, rotameters was the carrier gas.

Use of the higher-order Tyndall spectra (HOTS) and their dependence on particle size provided a simple method of checking for both particle size and homogeneity of particle size. An "OWL" was built to monitor the NaCl aerosol.

Suspended particles in a gas scatter, reflect, and absorb radiation to a degree depending on their size and shape and the nature and wavelength of the incident light. If a beam of light is passed through an aerosol and viewed at an angle against a dark background, the presence of particles is revealed by the scattered light giving rise to the "Tyndall beam". When white light is incident, a polydisperse aerosol will exhibit a blue Tyndal beam at all angles of observation from 0° to 180°.

For monodisperse aerosols, as the angle of observation varies from 0° to 180°, the sequence of colors follows the natural spectrum in the

order violet, blue, green, yellow, orange, and red. The brightness of the colors increases with the uniformity of particle size, and the number of times the spectral series is repeated increases with particle size. At angles where the intensity of the red scattered light is greater than the green, the scattered light appears red in color. Unless the aerosol is especially uniform in size, it is easier to identify the number of spectra from the number of "reds" present (8).

Determinations of the number of "reds" and the angle of appearance of the first red is best made in the chamber of an instrument known as the "OWL". The aerosol cloud is illuminated by parallel rays of white light; observation is made via a rotating telescope set on a protractor.

The aerosol was monitored in the OWL until the HOTS appeared. The very concentrated aerosol was then fed along with dry air into a dilution chamber. Here the concentration was reduced to a level which would not clog either the particle mass monitor or the diffusion plates. Baffles in the dilution chamber insured good mixing. Aerosol was withdrawn at the rate of 1.0 liter per minute for diffusion measurements at a point 110 centimeters down the dilution chamber.

In order to measure particle size independently of the diffusion mechanism, an aerosol centrifuge described by Bosco (11) was used. This high speed centrifuge (10,000 rpm) deposits aerosol particles on a calibrated foil scale. The deposition length of the particles is proportional to the aerodynamic diameter, d_{ae}. To convert to optical diameter, the following equation was employed (12).

$$\rho = \left(\frac{d_{ae}}{d_{op}}\right) \qquad (10)$$

Data Acquisition

For the room temperature measurements, the diffusion battery was suspended in ambient air and the sample ports were connected to the manifold, allowing sampling from one of the five sample ports. Aerosol was withdrawn from the first port (initial concentration N_o) until a relatively stable concentration had been reached. Then, consecutive 100-second samples were taken from each of the five ports. A sixth port was included in the manifold; it allowed dry air to enter the particle mass monitor.

The clean, dry air contributed no particle mass to the sensory crystals. Therefore, the frequency in the mixing circuit remained constant when the dry air was passing through the particle mass monitor. This allowed a continuous check on the background air and the performance of the instrument. Also, the clean air swept clear the connecting tubes preparing the mass monitor for the next aerosol sample.

Since the initial concentration, N_o, seen by the diffusion battery had to be known quite accurately, every other sample period was used for measuring N_o. Minor fluctuations in the air supply pressure (dilution air) and the expected 5 to 10 percent per hour decrease in the mass of aerosol generated were responsible for the variation observed in the N_o value.

Even numbered sample periods were used to follow the concentration of the aerosol as it left each diffusion plate, N_1, N_2, N_3, and N_4, respectively.

For low-temperature measurements, the diffusion battery was lowered into the insulated bath. The sample ports were connected to the manifold

and the sampling performed as before. Two low-temperature baths were employed. Ice and acetone were combined to produce temperature of -16 °C. Dry ice (CO_2(s)) and acetone were combined to produce the lowest temperature, -72 °C. The solid phase was always maintained in the baths. Once the diffusion battery was placed into a bath and was cooled to the bath temperature, the temperature in the insulated container remained constant for the duration of the experiment.

Data Analysis

To convert the frequency change of the mixer circuit into concentration ($\mu gm/m^3$), Equation (9) is recommended by the particle mass monitor manufacturer. The concentration is found by using the total frequency change Δf over any time interval Δt. The initial concentration, N_o, and the concentration of the aerosol leaving each plate was then plotted as a function of time and a concentration curve drawn for each diffusion plate assuming a constantly increasing or decreasing concentration during the time interval of the sampling.

To obtain the experimental value of penetration, N_i/N_o, the values of N_o and N_i were noted at any specific time on the curves described above. The penetration of the NaCl particles was calculated from the values of N_o, N_1, N_2, N_3 and N_4 obtained from the graph.

To compare the experimental penetration to the theoretical penetration, the experimental values must be plotted on the penetration curves previously calculated (Figure 2). Figure 8 shows how the data appear.

Since it was desired to compare not only the penetration but also the value of the diffusion coefficient, D, the value of D_{ex} must be obtained from the experimental penetration. Equation (3) (Figure 1) related

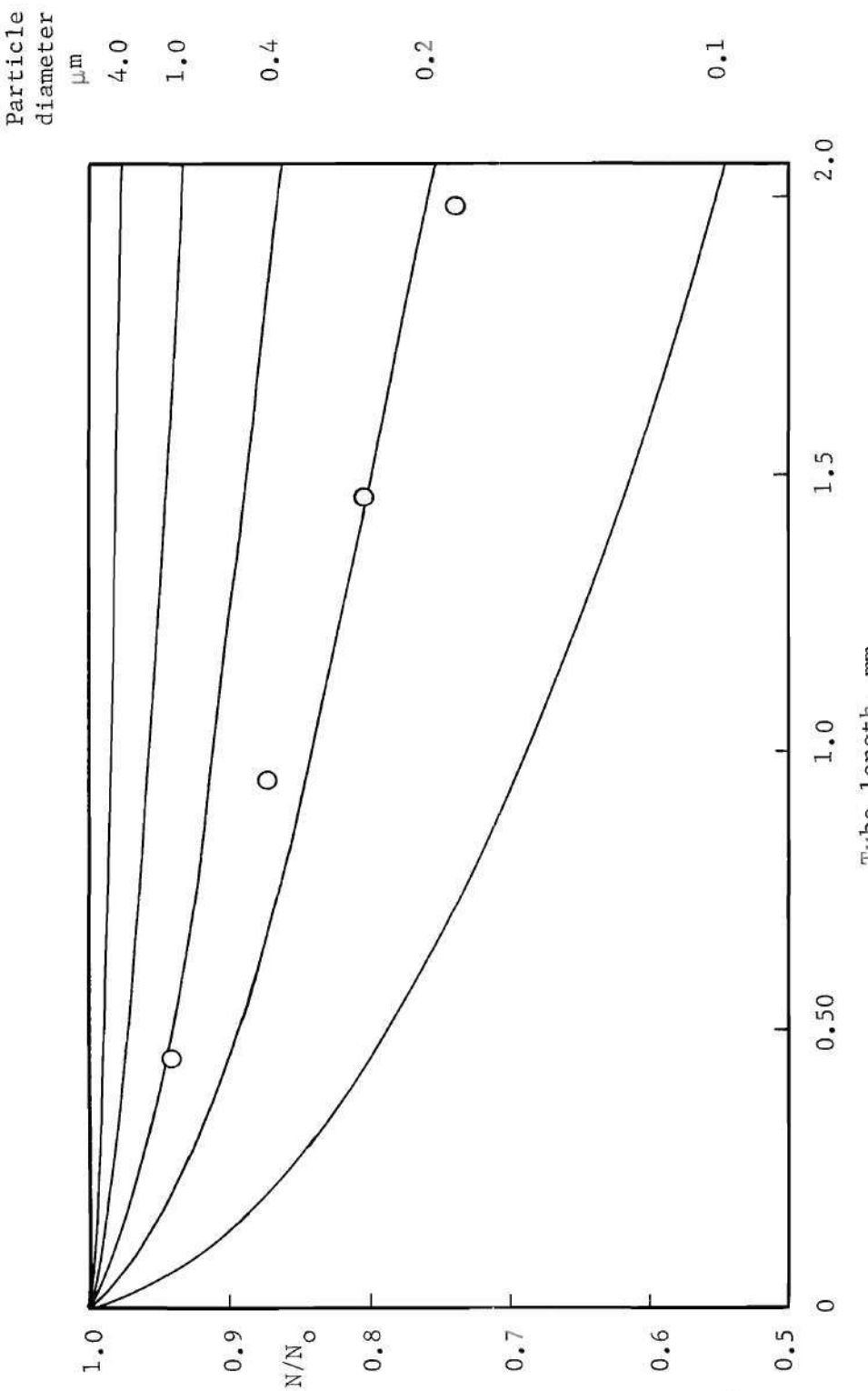

Figure 8. Graphical Comparison of Theoretical and Experimental Penetration

the penetration to Δ where

$$\Delta = \frac{Dx}{R^2 \bar{u}} \tag{11}$$

Solving for D, gives

$$D = \frac{\Delta R^2 \bar{u}}{x} \tag{12}$$

Therefore, the penetration values just calculated can be taken to Figure 1 to give a value of Δ. The value of D_{ex} is then obtained using Δ along with the known values of R^2, $\bar{u}$, and x. Comparison of this value with the theoretical value of D, Equation (8), permits determining the magnitude and the direction of the variation of the diffusion coefficient with temperature.

CHAPTER IV

PRESENTATION OF RESULTS

The diffusion experiments were conducted with two different diffusion battery arrangements. In the first, the work was done at room temperature (22°C) using as the four diffusion battery sections two nominal 125 micrometer CHS and two nominal 12.5 micrometer CHS, respectively. In the second, four nominal 12.5 micrometer CHS were used in work at both room temperature and at two other temperatures, -15 and -72°C.

Figures 9 and 10 show representative data from the first arrangement. In Figure 9, concentration changes after each plate are recorded. In Figure 10, only concentration after the 12.5 micrometer CHS is followed, but the period of observation has been greatly increased. Complete data for the first effort may be found in Appendix B.

Figure 11 shows the data points for all tests plotted of the theoretical curves. The runs may be grouped according to evaporator temperature: 860°C, 820°C, and 800°C.

From Figure 9, it is quickly concluded that the two 125 micrometer CHS have essentially no effect on the aerosol concentration. After many sets of experimental data showed this to be true, the conclusion was assumed to be valid. Therefore, experimental tests using three evaporator temperatures have effectively only two sets of data points. More than two sets of points are needed, however, to permit drawing reliable conclusions from data such as these.

As a result, two more of the nominal 12.5 micrometer CHS were

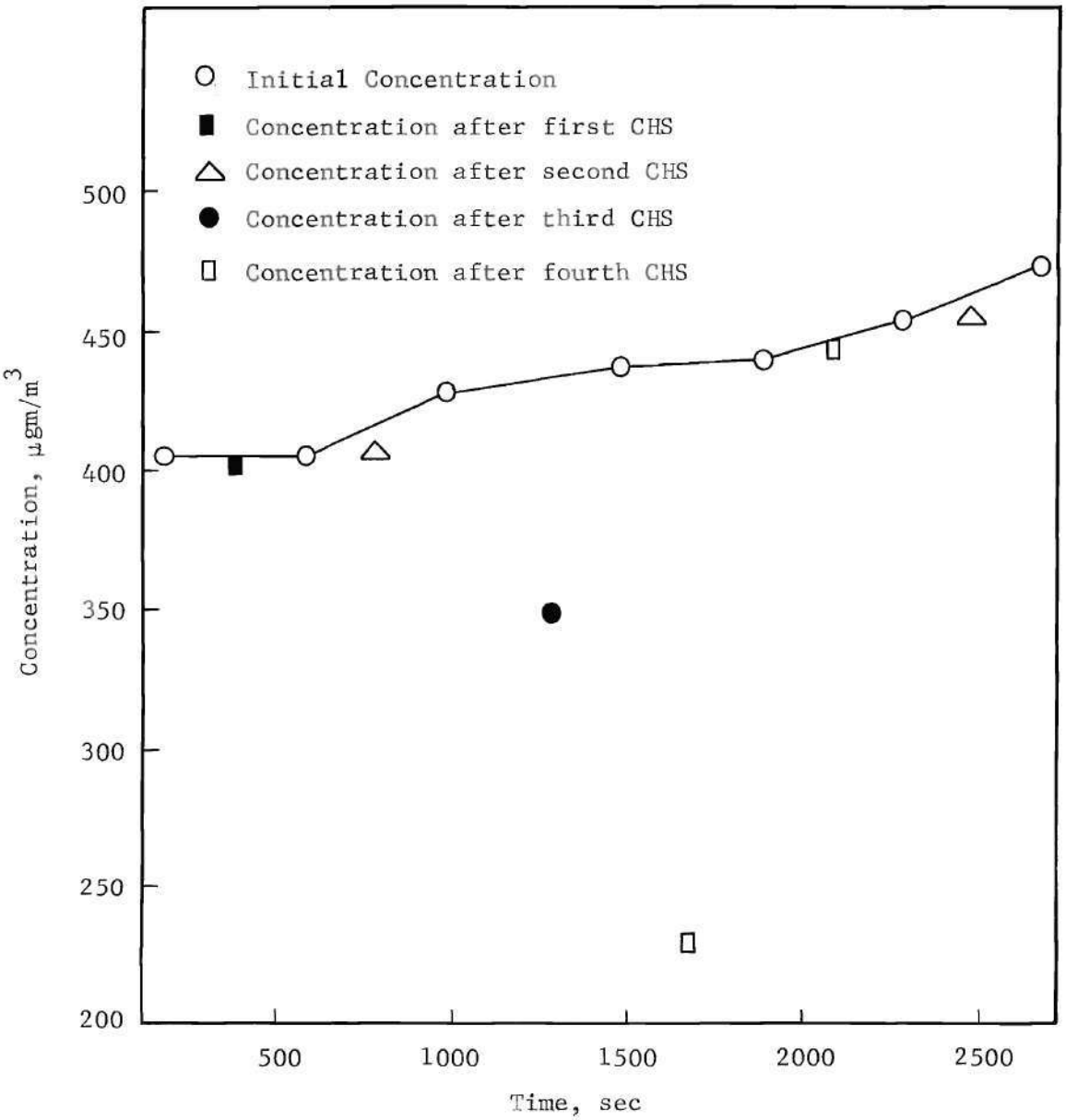

Figure 9. Sample Concentration Data: Two 125 Micrometer and Two 12.5 Micrometer Diameter CHS

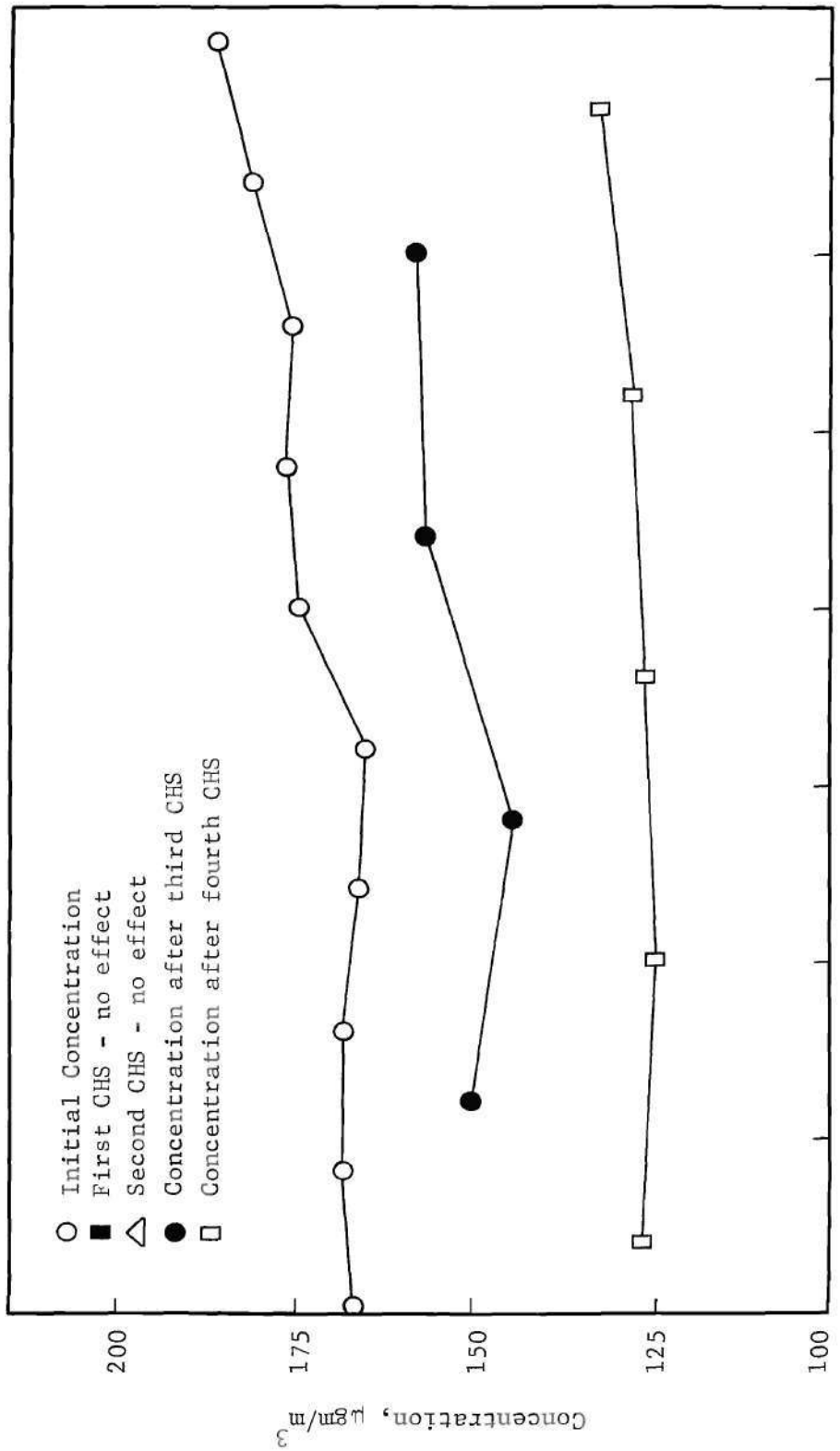

Figure 10. Concentration Changes of Nacl Aerosol Passing Through Four CHS: Two of 125 Micrometer and Two of 12.5 Micrometer Diameter

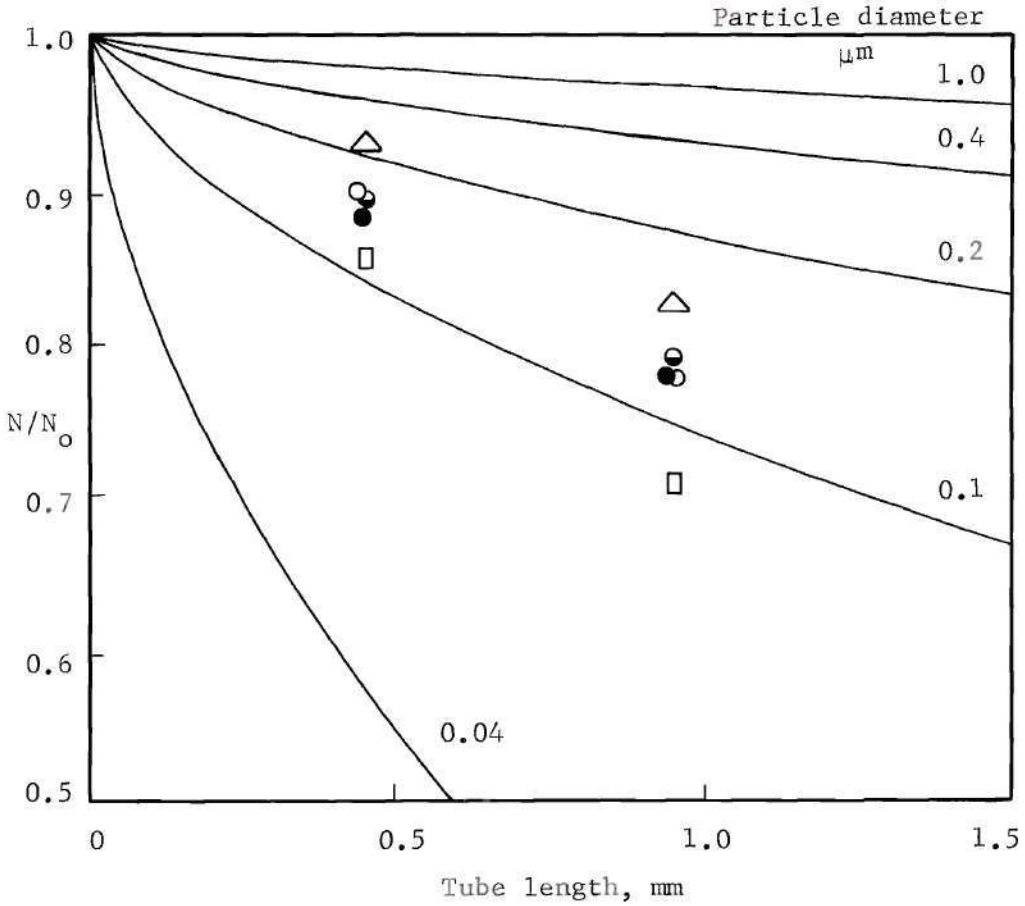

Experimental data	Evaporator Temperature
□	800 °C
◒ ○ ●	820 °C
△	860 °C

Figure 11. Penetration of NaCl Aerosol: Two 125 Micrometer and Two 12.5 Micrometer Diameter CHS in Series

obtained and the second arrangement for experimentation was begun. Figure 12 shows representative data from the room temperature part of this effort. The concentration of NaCl aerosol leaving each plate produces a definite trend, but a very long period of observation was necessary to insure that the data obtained was useful and reliable. Complete data may be found in Appendix C. Figures 13, 14, and 15 compare the experimental data from the 22 °C, -16 °C, and -72 °C tests, respectively, to the theoretically predicted curves.

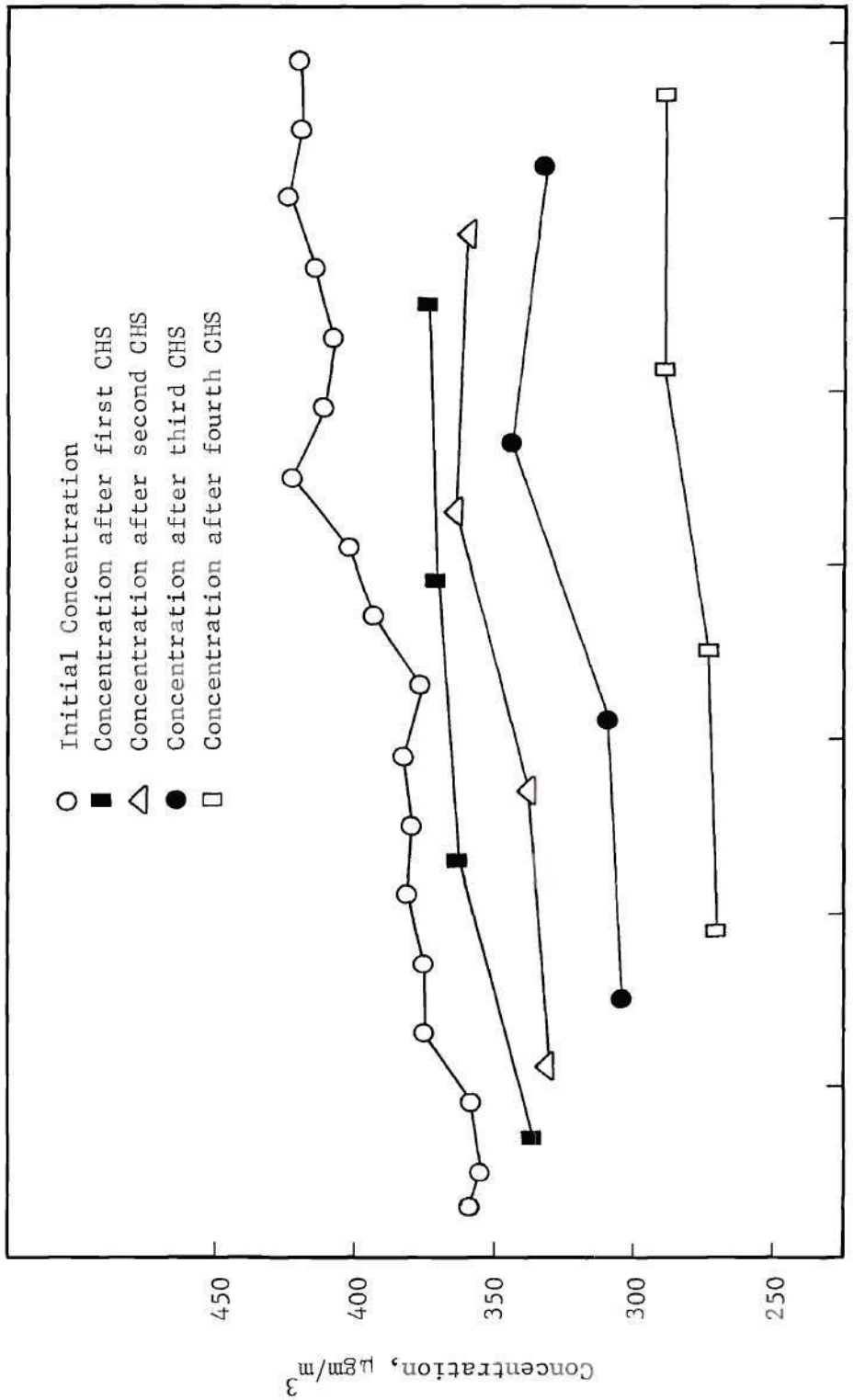

Figure 12. Concentration Change of NaCl Aerosol Passing Through Four 12.5 Micrometer Diameter CHS

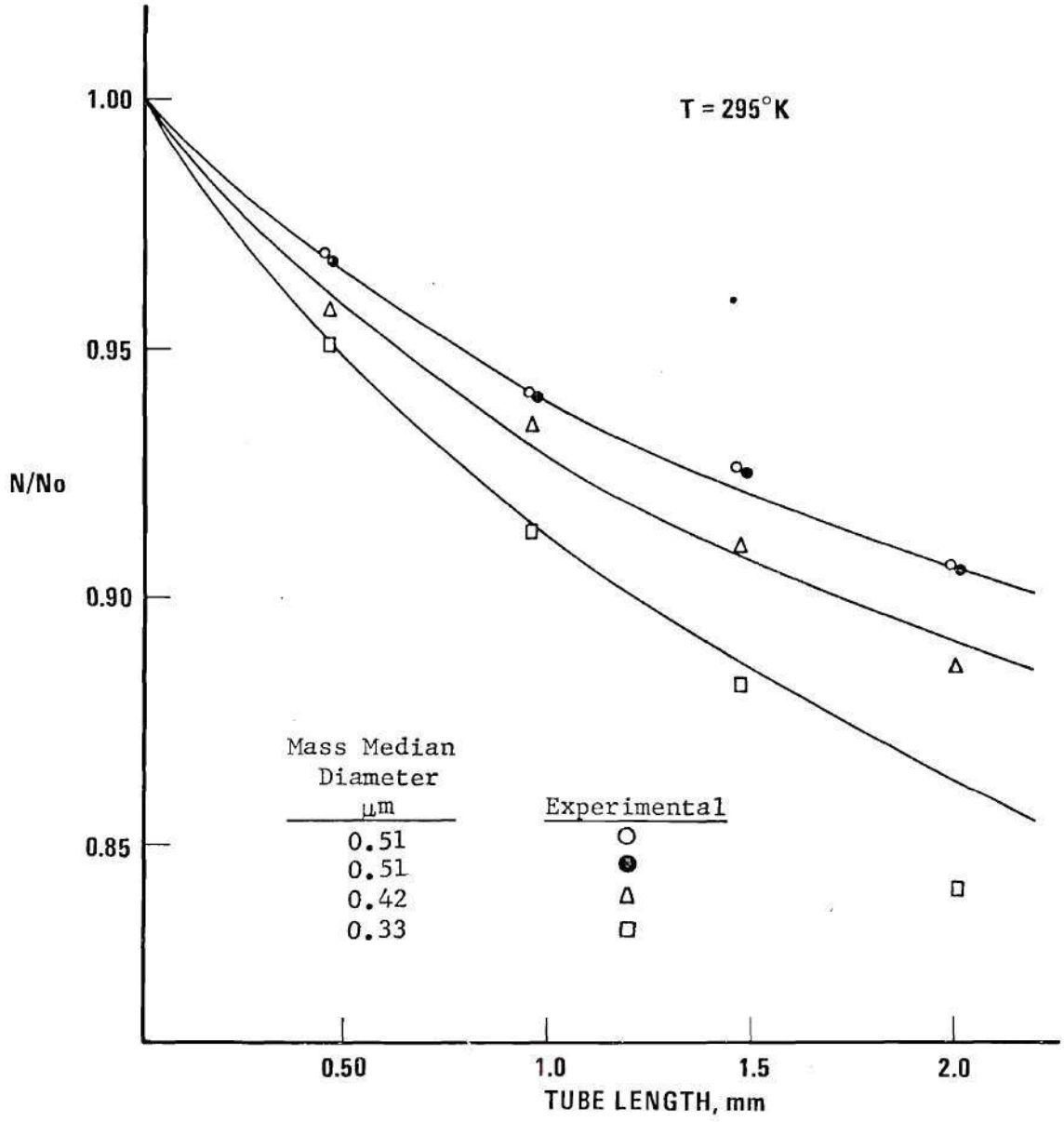

Figure 13. Penetration of NaCl Aerosol: Four 12.5 Micrometer CHS in Series, T = 295 °K

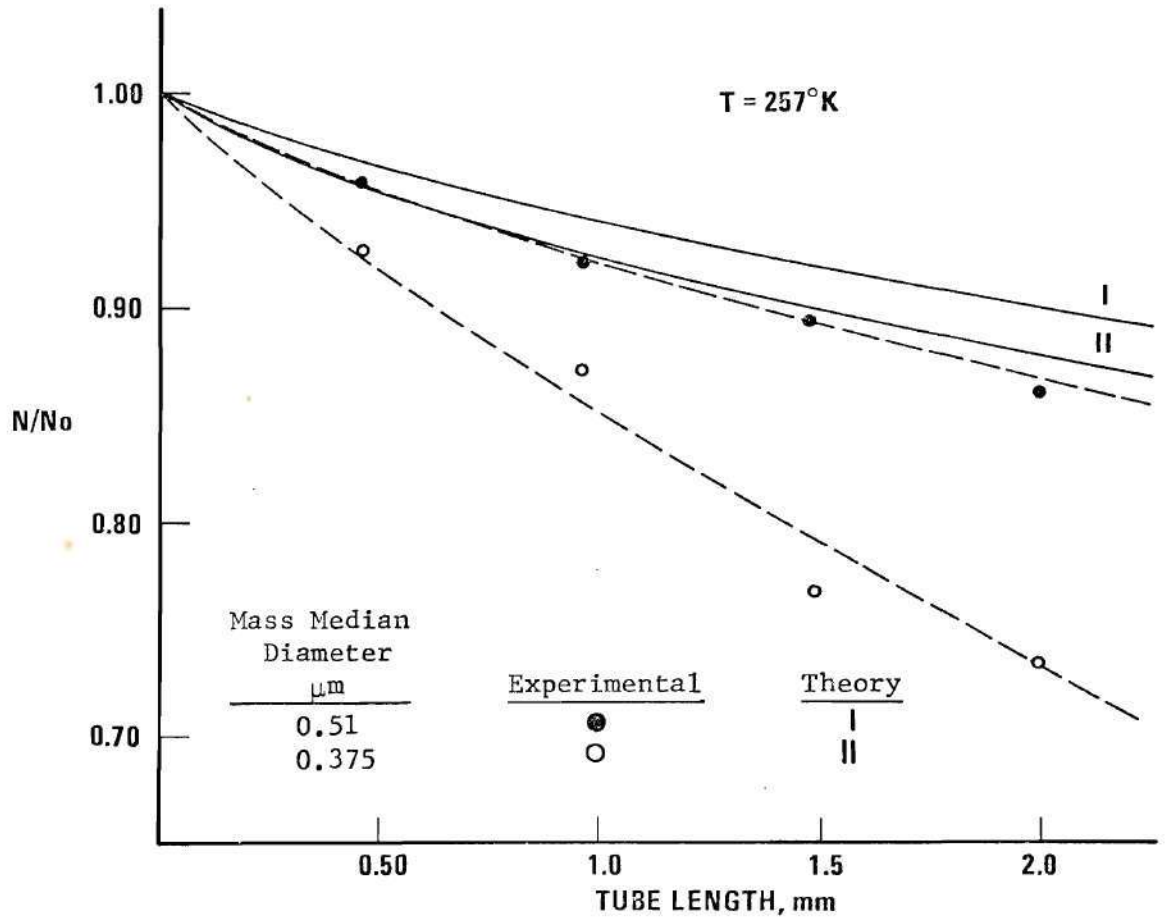

Figure 14. Penetration of NaCl Aerosol: Four 12.5 Micrometer CHS in Series, T = 257 °K

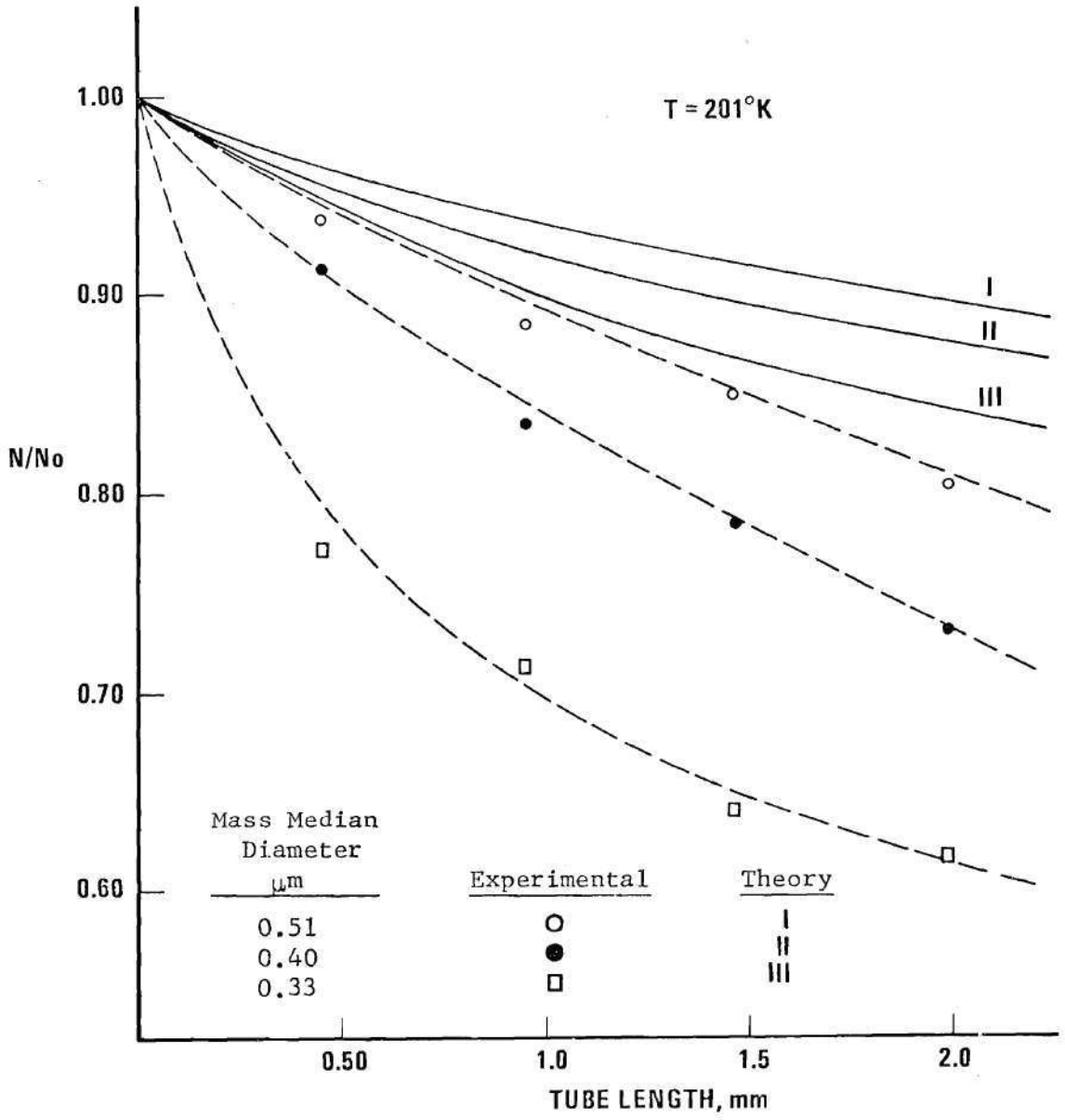

Figure 15. Penetration of NaCl Aerosol: Four 12.5 Micrometer CHS in Series, T = 201 °K

CHAPTER V

DISCUSSION OF RESULTS

Since the diffusion of aerosol particles within the battery is sensitive to the uniformity of the hole diameter and length in the collimated hole structures, it was necessary to verify these dimensions for each plate. The plates were photographed using a transmission electron microscope; the photographs of the holes were analyzed with the Zeiss, TGZ 3, Particle Size Analyzer. A micrometer was used to find the plate thickness. These results are presented in the following Table.

Table 1. CHS Dimensions

Plate	Mean Diameter μm	Standard Deviation μm	Plate Thickness in
1	131.4	12.27	0.0485
2	131.1	9.86	0.0460
3	16.05	3.86	0.0185
4	15.09	3.74	0.0200
5	15.51	3.79	0.0205
6	15.20	3.51	0.0210

The holes examined were not circular and exhibited rather rough edges. This contributes to an increase in the area available for deposition and makes the holes have effectively a smaller diameter. The holes were treated as circles of equivalent cross-sectional area in determining the mean diameter.

Analysis of the diffusion data must start with Figure 9. Here it is clearly seen that the larger (125 micrometer) CHS have a neglible

effect on the aerosol deposition. While the hole diameter is certainly small enough for diffusion to be a factor, the tube length of the CHS (1.25 millimeter) is far too short for Brownian motion to have any real effect.

Figure 12 shows diffusion as a function of length when the two 125 micrometer CHS have been neglected. The figure shows the decrease in aerosol particle size with a decrease in the evaporator temperature of the aerosol generator. Since there are only two data points on each curve, no other conclusions regarding diffusion theory should be drawn.

Results of passing the test aerosol through four plates with a nominal hole size of 12.5 micrometer, however, show a definite continuous loss of particles. These data were reproducible with a maximum variation of 20 percent.

The small variations from one experimental run to the next (Figure 13) must be due to small changes in the aerosol particle size. No two tests were made during exactly the same time period following the insertion of the dry solid NaCl into the evaporation heater of the aerosol generator. Normally a 5 to 10 percent per hour decrease in the concentration of the aerosol leaving the LaMer generator would be expected. Since particle size is related to concentration, it would also be expected that the particle size should decrease. An aerosol centrifuge (11) was used to check the change in aerosol particle size during a test. The change found in the aerodynamic diameter of the NaCl particles is given in Table 2.

Table 2. Effect of Time on NaCl Particle Size

Time, hr	d_{ae}, μm	d_{op}, μm
0	.62	.421
3	.59	.401
6	.57	.388

The NaCl was inserted into the heater about 20 minutes prior to the first sampling. This 1.1 to 1.7 percent per hour change in particle size would not significantly affect a single experimental test, but it would affect three consecutive tests based on the same NaCl charge.

From the raw experimental data (Appendix E), it can easily be seen that more particles are removed from the air stream than theory predicts. The theory, derived by Gormley and Kennedy (5), is based on the following assumptions:

(1) the aerosol is homogeneous with respect to particle size,

(2) all particles which contact the walls of the channel adhere,

(3) the effect of turbulence in the entrance of the channels is negligible,

(4) the pressure drop across the battery is small,

and (5) diffusion of the particles is not affected by electrostatic charges on the particles or battery walls.

Tests with the aerosol centrifuge showed that the aerosol particles were close to being homogeneous. However, the size distribution became more skewed toward the small particles as time increased. Since smaller particles diffuse more rapidly than large ones, more diffusion will occur than would be predicted using the average particle size for these cases.

This effect will be most important as the length of time since insertion of solid NaCl into the LaMer generator becomes very large (e.g., 8-9 hours).

During this time period, a systemic error may be introduced also. The particle mass monitor counts the total mass passing through the diffusion battery; it may be applied to this type experiment only when a monodisperse aerosol is used. In a monodisperse aerosol, the mass of the particles is directly proportional to the number of particles, (total mass/mass of single particle = total number of particles). If the aerosol size distribution is skewed toward the smaller particles, there will be more particles present than would be predicted by dividing the total mass by the mass of a single particle having the mean diameter.

All the aerosol particles that contact the walls of the tubes undoubtedly adhere. However, some particles impact the face of the CHS and are also removed from the air stream. These losses are not taken into account by the diffusion theory of Gormeley and Kennedy.

This partial efficiency of impaction, ϵ_i, is given by the equation of Pich (13)

$$\epsilon_i = \frac{2\,\epsilon_i'}{1+\xi} - \frac{\epsilon_i'^{\,2}}{(1+\xi)^2} \qquad (13)$$

where

$$\epsilon'_i = 2\,\mathrm{Stk}\,\sqrt{\xi} + 2\,\mathrm{Stk}^2 \exp\left[-\frac{1}{\mathrm{Stk}\sqrt{\xi}}\right] - 2\,\mathrm{Stk}^2\xi \qquad (14)$$

$$\xi = \frac{\sqrt{P}}{1-\sqrt{P}} \qquad (15)$$

$P = A_p/A_f$

A_p = area of pores, cm^2

A_f = area of filter, cm^2

Stk = Stokes' number

$$Stk = \frac{mq}{6\pi r R_o} \tag{16}$$

m = mass of single particle, gm

q = face velocity of gas, cm/sec

r = radius of particle, cm

and R_o = pore radius, cm

Impaction efficiency was calculated for the experimental flow conditions and particle sizes with the results shown in Table 3.

Table 3. Impaction Efficiency- A Function of Temperature and Particle Size

r, μm	295°K	257°K	201°K
.51	.0944	.0892	.0842
.455	.0763	.0722	.0679
.40	.0605	.0571	.0537

The impaction efficiency is additive with the diffusion efficiency, ϵ_D, to give the total efficiency of removal, E. When negligibly small terms are eliminated, the final expression is (13)

$$E = \epsilon_i + \epsilon_D \tag{17}$$

The loss of particles by impaction would be expected to occur for each plate and the effect is therefore cummulative.

When the experimental data are corrected for the impaction loss, the diffusion measurements predict the following values for the diffusion coefficient.

Table 4. Experimental Diffusion Coefficient

Particle Size, μm	D_{Th}	Experimental D at each Plate 1	2	3	4
T = 295°K					
.42	7.8×10^{-7}	8.94×10^{-7}	7.12×10^{-7}	7.64×10^{-7}	9.35×10^{-7}
.51	6.1×10^{-7}	5.62×10^{-7}	6.21×10^{-7}	5.84×10^{-7}	6.09×10^{-7}
.33	1.07×10^{-6}	1.129×10^{-6}	1.071×10^{-6}	1.17×10^{-6}	1.415×10^{-6}

Particle Size, μm	D_1/D_{Th}	D_2/D_{Th}	D_3/D_{Th}	D_4/D_{Th}
.42	1.14	.91	.98	1.20
.51	.92	1.02	.98	1.0
.33	1.05	1.0	1.09	1.3

T = 257°K Particle Size, μm	D_{Th}	Experimental D at each Plate			
.51	5.60×10^{-7}	7.78×10^{-7}	8.12×10^{-7}	8.7×10^{-7}	9.92×10^{-7}
.375	8.20×10^{-7}	1.765×10^{-6}	1.77×10^{-6}	3.28×10^{-6}	3.01×10^{-6}

Particle Size, μm	D_1/D_{Th}	D_2/D_{Th}	D_3/D_{Th}	D_4/D_{Th}
.51	1.39	1.45	1.55	1.77
.375	2.15	2.16	4.10	3.67

T = 201°K Particle Size, μm	D_{Th}	Experimental D at each Plate			
.51	4.90×10^{-7}	1.113×10^{-6}	1.179×10^{-6}	1.239×10^{-6}	1.405×10^{-6}
.40	6.60×10^{-7}	1.76×10^{-6}	2.075×10^{-6}	2.32×10^{-6}	2.425×10^{-6}

Table 4. (Continued)

T = 201°K Particle Size, μm	D_{Th}	Experimental D at each Plate			
.30	9.60×10^{-7}	8.8×10^{-6}	5.52×10^{-6}	5.55×10^{-6}	4.42×10^{-6}
Particle Size, μm	D_1/D_{Th}	D_2/D_{Th}	D_3/D_{Th}	D_4/D_{Th}	
.51	2.27	2.40	2.52	2.87	
.40	2.67	3.14	3.51	3.67	
.30	9.17	5.75	5.78	4.60	

Diffusion coefficients calculated from tests made at room temperature are very close to the theoretical diffusion coefficient. The experimental values given in Table 4 are within ± 10 percent with a single exception on CHS number 4. On plate 4, the predicted value is high by about 20 percent.

At 257°K (-16°C), the diffusion coefficient predicted by experiment is markedly higher than theoretical values. Diffusion experiments yield values that are 30-100 percent higher. This means that diffusion is occurring more rapidly than would be expected for any given particle size.

At 201°K (-72°C), the difference between experment and theory is even more marked. Diffusion measurements yield diffusion coefficient values that are 150-475 percent higher than the theoretically predicted ones. Thus, at this rather low temperature, diffusion is occurring much more rapidly than theory would predict. The system is behaving as if particles 50-65 percent smaller in diameter than those actually observed were present.

Since the experimental data correlated so well with theoretical predictions for the room temperature measurements, the error introduced into the system by using the particle mass monitor instead of a particle counter must be small. The aerosol, then, as it appears to the system, must be essentially monodisperse.

Explanation of such a deviation from theory must come from the manner in which the theory was derived, since it appears that the physical makeup of the system has been the same for all the different temperatures. All diffusion theory--from Einstein to Gormley and Kennedy--has been derived assuming that the gas in the aerosol system was ideal. At room temperature, this is a very good assumption. However, at low temperatures, deviations from ideal behavior apparently have become serious enough to affect the diffusion rate.

At low temperatures, there are more molecules per unit volume. In like manner, there are more gas molecules per aerosol particle. While the thermal energy of an individual gas molecule is less, there are more collisions between gas molecules and aerosol particles per unit time; the mean free path of the gas molecules is smaller. The distribution of the speeds of the gas molecules becomes more narrow also. Therefore, the chance of radical random motion is small. Statistically, the chance for a great many equal "pushes" on the aerosol particle by the surrounding gas molecules is great.

As the aerosol particles near the tube wall, the greater attractive force between gas molecules at the lower temperatures may become important. The gas molecules close to the wall are "drawn" toward the bulk of the gas stream. This will leave a net force driving the aerosol particles toward the wall.

CHAPTER VI

CONCLUSIONS

The following conclusions can be drawn from the experimental results:

1. Collimated Hole Structures can be used to construct a compact and inexpensive diffusion battery that will yield reproducible diffusion measurements.

2. The diffusion of a NaCl aerosol at room temperature (22 °C) correlates well with diffusion theory as derived by Gormley and Kennedy.

3. The diffusion of aerosols is altered at low temperatures; at -16 and -72 °C, the effective diffusion coefficient is 2 to 4 times the value that would be predicted by present theory.

4. Diffusion theory, as developed using the assumption of an ideal gas, accurately predicts the diffusion of aerosols at room temperature. At low temperatures, the more non-ideal the gas, i.e., the colder the aerosol, the more incorrect is present diffusion theory.

CHAPTER VII

RECOMMENDATIONS

The following recommendations can be made as a result of this work:

1. Diffusion measurements should be extended to temperatures below -72 C.

2. The use of both the particle mass monitor and a condensation nuclei counter is recommended in further low temperature diffusion work so that the actual number of particles as well as the mass of the particles may be found.

3. The use of polystyrene latex spheres of various sizes is recommended in further diffusion work. These spheres give an aerosol that is more nearly monodisperse. They will permit determining if various size particles are affected differently at low temperatures.

4. Some evidence from this work suggests that the diffusion of aerosols at low temperature is affected by the concentration of the aerosol. Therefore, more work in this area is recommended.

APPENDICES

APPENDIX A

CHS AND DIFFUSION BATTERY DATA

Table 5. Size Analyzer Data

CHS	Total Holes	Magnification	Channel Number	Holes Counted
1	992	32X	17	0
			18	1
			19	20
			20	215
			21	405
			22	294
			23	51
			24	6
			25	0
2	1076	32X	18	0
			19	9
			20	228
			21	523
			22	272
			23	42
			24	2
			25	0
3	1008	280X	17	0
			18	4
			19	19
			20	89
			21	142
			22	218
			23	217
			24	154
			25	100
			26	44
			27	9
			28	9
			29	3
			30	0
4	1024	280X	16	0
			17	16
			18	54

Table 5. (Continued)

CHS	Total Holes	Magnification	Channel Number	Holes Counted
			19	99
			20	186
			21	239
			22	168
			23	131
			24	86
			25	37
			26	6
			27	2
			28	0
5	1108	198X	10	0
			11	3
			12	31
			13	129
			14	249
			15	298
			16	241
			17	119
			18	26
			19	9
			20	3
			21	0
6	1148	198X	10	0
			11	7
			12	42
			13	160
			14	324
			15	326
			16	200
			17	66
			18	17
			19	6
			20	0

Table 6. Conversion of Size Analyzer Data Considering Magnification

32X	Zeiss Manuel		Channel Number	Calculated Diameter	
	Mean	Limits		Mean	Limits
		3.53 mm			110.31250 μm
	3.62		18	119.0625	
		3.72			116.250
	3.81		19	119.0625	
		3.90			121.8750
	3.99		20	124.6875	
		4.08			127.50
	4.18		21	130.625	
		4.27			133.4375
	4.36		22	136.250	
		4.45			139.0625
	4.54		23	141.875	
		4.64			145.00
	4.73		24	147.8125	
		4.82			150.625
280X		3.35			11.9642
	3.44		17	12.2857	
		3.53			12.6071
	3.62		18	12.9285	
		3.72			13.2857
	3.81		19	13.6071	
		3.90			13.9285
	3.99		20	14.2500	
		4.08			14.5714
	4.18		21	14.9285	
		4.27			15.250
	4.36		22	15.5714	
		4.45			15.8928
	4.54		23	16.2142	
		4.64			16.5714
	4.73		24	16.8928	
		4.82			17.2142
	4.91		25	17.5357	
		5.00			17.8571
	5.10		26	18.2142	
		5.19			18.5357
	5.28		27	18.8571	
		5.37			19.1785
	5.46		28	19.5000	
		5.56			19.8571
	5.65		29	20.1785	
		5.74			20.500

Table 6. (Continued)

32X	Zeiss Manuel		Channel Number	Calculated Diameter	
	Mean	Limits		Mean	Limits
		2.24 mm			11.31 μm
198X	2.34		11	11.82	
		2.43			12.27
	2.52		12	12.73	
		2.61			13.18
	2.70		13	13.64	
		2.80			14.14
	2.89		14	14.60	
		2.98			15.05
	3.07		15	15.50	
		3.16			15.96
	3.26		16	16.46	
		3.35			16.92
	3.44		17	17.37	
		3.53			17.83
	3.62		18	18.28	
		3.72			18.79
	3.81		19	19.24	
		3.90			19.70
	3.99		20	20.15	

Table 7. Velocity of Aerosol Through CHS

Plates	L/D	CHS Thickness .001 in	Hole Diameter μm	Number of Holes	Open Area
1	8.85	46	132	5500	50%
2	9.25	48		5500	50%
3	28.5	18.0	16.1	335,000	32%
4	33.7	20.0	15.1	335,000	32%
5	33.6	20.5	15.5	335,000	32%
6	34.9	21.0	15.3	335,000	32%

Flow through CHS Tubes when campling 1 L/min

$$\bar{U} = \frac{Q}{A} = \frac{cm^3/min}{cm^2}$$

$$Q = 1000\ cm^3/min \cdot min/60\ sec = 16.67\ cm^3/sec$$

$$A = \frac{\pi D^2}{4} \cdot .32 = .6329\ cm^2$$

$$\bar{U} = \frac{16.67}{.6329} = 26.33\ cm/sec$$

for plates 3, 4, 5, and 6

$$Q = 16.67\ cm^3/sec$$

$$A = \frac{\pi D^2}{4} \cdot .50 = .9890\ cm^2$$

$$\bar{U} = \frac{16.67}{.9890} = 16.85\ cm/sec$$

for plates 1 and 2.

Table 8. Reynolds' Number Calculation

$$N_{Re} = \frac{D\bar{u}\rho}{\mu}$$

D = dia, cm

u = velocity, cm/sec

μ = viscosity, of air, cp

ρ = density, of air, gm/cm^3

T = 21°C

D = 14.57×10^{-4} cm

u = 26.33 cm/sec

μ = 1.78×10^{-4} gm/cm.sec

ρ = .00117 gm/cm^3

N_{Re} = .025

T = -70°C

D = 14.57×10^{-4} cm

u = 18.3 cm/sec

ρ = .00168 gm/cm^3

μ = 1.38×10^{-4} gm/cm.sec

N_{Re} = .0324

Table 9. Pressure Drop Through Diffusion Battery

Volume of Air, cm^3/min	Pressure Drop, in of H_2O	Volume of Air cm^3/min	Pressure Drop in of H_2O
Flow through 4 plates		Flow through 2 plates	
780	4.56		
780	4.56		
710	4.17	890	2.48
720	4.23	890	2.47
720	4.23	770	2.11
620	3.67	770	2.10
630	3.70	630	1.70
640	3.72	630	1.71
640	3.71	520	1.39
490	2.88	520	1.39
490	2.90		
490	2.89		
340	2.04		
340	2.04		
Flow through 3 plates		Flow through 2 plates	
890	3.87	520	0.56
890	3.88	530	0.56
780	3.40	700	0.79
790	3.42	700	0.79
790	3.41	830	0.99
660	2.85	840	0.97
660	2.84	840	0.97
530	2.25	990	1.19
530	2.25	990	1.19

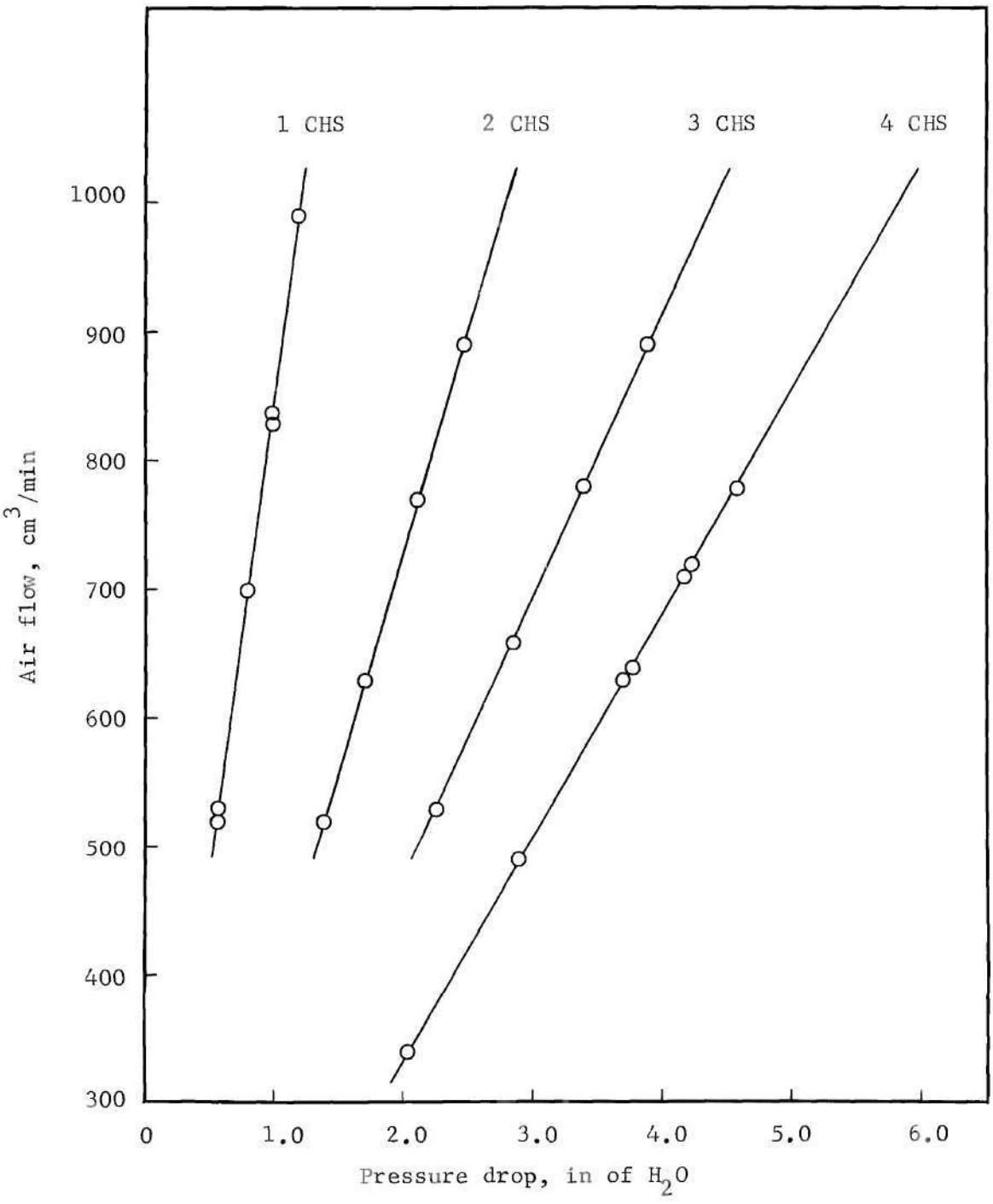

Figure 16. Pressure Drop Through Diffusion Battery

APPENDIX B

THEORETICAL DIFFUSION COEFFICIENT

$$D = B\ kT$$

where k = Constant

T = temperature, °K

$$B = (1 + A\ \ell/r + Q\ \ell/r \exp^{[-\frac{br}{\ell}]})/6\pi\eta r$$

A = 1.246

Q = .42

b = .87

Table 10. D_{Th} at 295 °K

T = 295°K $\quad \ell = .064$ $\quad \eta = .0177$ cp

d, μm	B	D
1	.0695	2.775×10^{-7}
.4	.2109	8.422×10^{-7}
.2	.5594	2.233×10^{-6}
.1	1.7188	6.862×10^{-6}

Table 11. D_{Th} at 257°K

T = 257° K		ℓ = .056 η = .0163 cp
d, μm	B	D
1	0.741	2.588×10^{-7}
.4	0.2203	7.690×10^{-7}
.2	.5687	1.985×10^{-6}
.1	1.700	5.933×10^{-6}

Table 12. D_{Th} at 201°K

T = 201° K		ℓ = .044 η = .0139
d, μm	B	D
1	.0847	2.300×10^{-7}
.4	.2434	6.612×10^{-7}
.2	.6006	1.631×10^{-6}
.1	1.705	4.631×10^{-6}

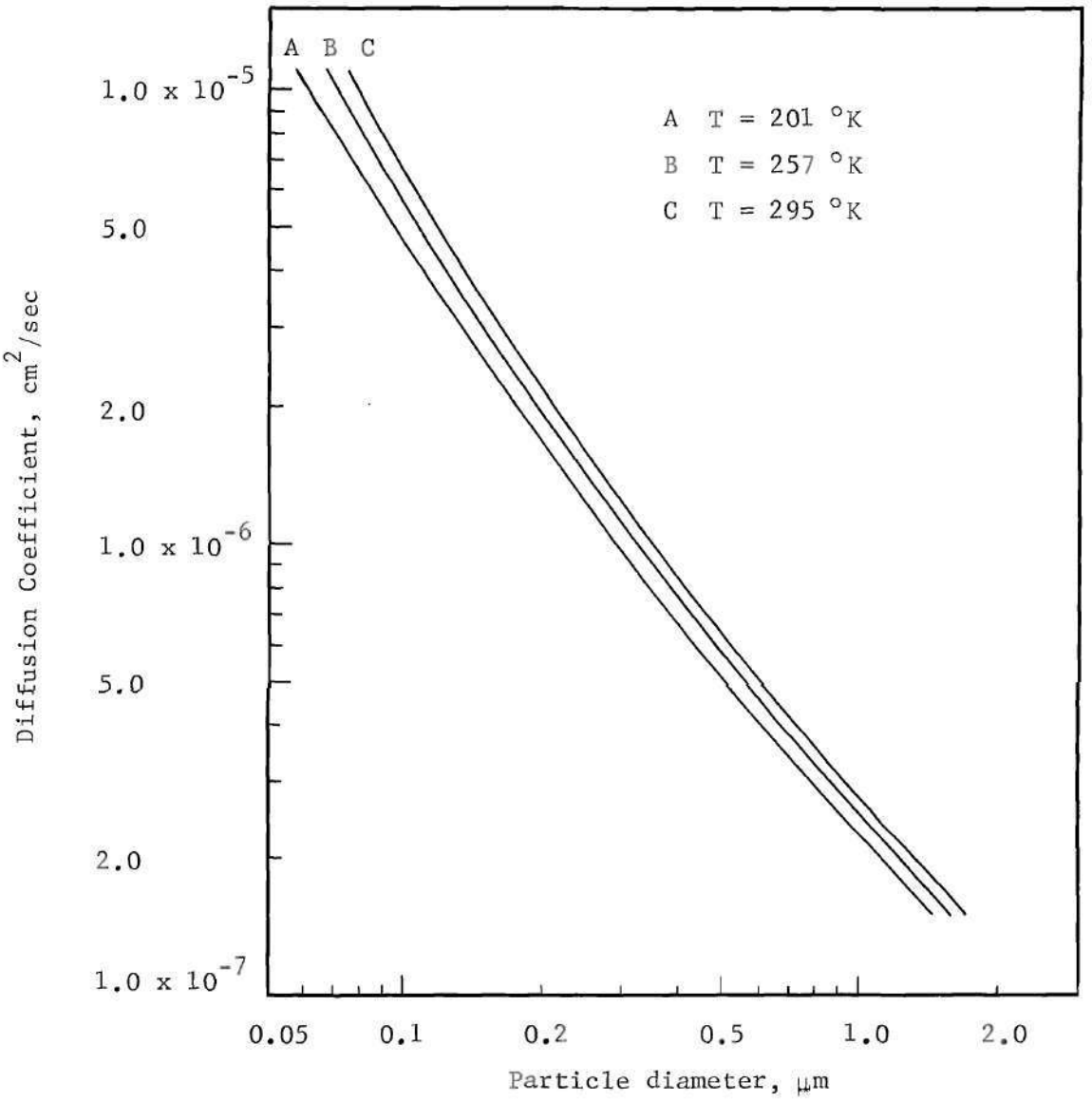

Figure 17. Theoretical Diffusion Coefficient

APPENDIX C

THEORETICAL CALCULATIONS

Table 13. Theoretical Penetration for a Given Particle Size

$$\Delta = \frac{Dx}{R^2 u}$$

Tube dia, μm	Total Length, .001 in.
16.1	18
15.1	38
15.5	58.5
15.3	79.5

$T = 295^{\circ}K$

$\bar{U} = 26.33$ cm/sec

d, μm	D_{Th}	1	2	3	4
.51	6.1×10^{-7}	1.635×10^{-4}	3.92×10^{-3}	5.74×10^{-3}	8.02×10^{-3}
.42	7.8×10^{-7}	2.09×10^{-3}	5.02×10^{-3}	7.35×10^{-3}	1.025×10^{-2}
.33	1.07×10^{-6}	2.87×10^{-3}	6.87×10^{-3}	1.005×10^{-2}	1.405×10^{-2}

d, μm	1	2	3	4
.51	.968	.940	.824	.905
.42	.961	.930	.910	.890
.33	.951	.913	.889	.864

$T = 257^{\circ}K$

$\bar{U} = 22.9$ cm/sec

		Δ			
d, μm	D	1	2	3	4
.45	6.60×10^{-7}	2.035×10^{-3}	4.95×10^{-3}	7.14×10^{-3}	9.97×10^{-3}
.375	8.20×10^{-7}	2.53×10^{-3}	6.06×10^{-3}	8.87×10^{-3}	1.239×10^{-2}
.51	5.60×10^{-7}	1.725×10^{-3}	4.14×10^{-3}	6.06×10^{-3}	8.46×10^{-3}

	N/N_o			
d, μm	1	2	3	4
.45	.961	.930	.910	.890
.375	.955	.920	.900	.875
.51	.968	.940	.920	.900

$T = 201^{\circ}K$

$\bar{U} = 18.3$ cm/sec

		Δ			
d, μm	D	1	2	3	4
.40	6.60×10^{-7}	2.54×10^{-3}	6.1×10^{-3}	8.94×10^{-3}	1.25×10^{-2}
.51	4.90×10^{-7}	1.89×10^{-4}	4.53×10^{-3}	6.64×10^{-3}	9.26×10^{-3}
.30	9.60×10^{-7}	3.70×10^{-3}	8.88×10^{-3}	1.30×10^{-2}	1.815×10^{-2}

	N/N_o			
d, μm	1	2	3	4
.40	.055	.920	.899	.874
.51	.964	.935	.914	.895
.30	.942	.899	.870	.842

Table 14. Calculation of Impaction Efficiency

$$E_i = \frac{2\,\epsilon_i'}{1+\xi} - \frac{\epsilon_i'^2}{(1+\xi)^2}$$

where $\epsilon_i' =$

$$2\,Stk\sqrt{\xi} + 2\,Stk^2\sqrt{\xi}\exp\left[-\frac{1}{Stk\sqrt{\xi}}\right] - 2\,Stk^2\,\xi$$

and

$$\xi = \frac{\sqrt{P}}{1-\sqrt{P}}$$

and

$$Stk = \frac{mq}{6\eta r R_o}$$

where

m = mass of particle, gm

q = face velocity, cm/sec

η = viscosity, cp

r = particle radius, cm

R_o = tube radius, cm

and P = porosity of filter

Table 14. (Continued)

Particle, μm	T = 295°K			T = 257°K			T = 201°K		
	Stk	ϵ_i'	ϵ_i	Stk	ϵ_i'	ϵ_i'	Stk	ϵ_i'	ϵ_i
.4	.0249	.0593	.0475	.0235	.0522	.0448	.0220	.0490	.0421
.455	.0320	.0705	.0603	.0302	.0665	.0569	.0283	.0624	.0535
.51	.0403	.0877	.0747	.0379	.0828	.0706	.0355	.0778	.0665

APPENDIX D

CALCULATED DATA

Sample Calculations

From Figure 26, read value of N_o, N_1, N_2, N_3, and N_4. Find N_i/N_o.

Time, sec	N_o	N_1	N_1/N_o
900	250	227	.908
4500	246	225	.914
7300	246	225	.914
	N_o	N_2	N_2/N_o
3700	237.5	202	.851
6900	241	206.5	.858
8100	251.5	215	.855
	N_o	N_3	N_3/N_o
			.818
2900	237.5	180	.758
5300	244	192	.787
	N_o	N_4	N_4/N_o
5700	242.5	177	.730
6100	247.5	175	.722

$\overline{N_1/N_o}$ = .912 $\overline{N_3/N_o}$ = .788

$\overline{N_2/N_o}$ = .854 $\overline{N_4/N_o}$ = .726

Correct for ϵ_i of .045

ϵ_i 1 plate = .045

ϵ_i 2 plates = .09

ϵ_i 3 plates = .135

ϵ_i 4 plates = .18

N_1/N_o = .912/.955 - .958

N_2/N_o = .854/.910 = .936

N_3/N_o = .788/.865 = .911

N_4/N_o = .726/.820 = .886

Plot N_i/N_o values on Figure 13.

To compare the theoretical and experimental values of the Diffusion Coefficient, D, proceed as follows.

For the N_i/N_o values just found, read the corresponding Δ value from Figure 1.

N_i/N_o	Δ
.958	2.40×10^{-3}
.936	4.58×10^{-3}
.911	7.2×10^{-3}
.886	1.07×10^{-2}

Since $\Delta = \frac{D\,x}{R^2\,\bar{u}}$, one may now solve for D using the experimental value Δ just found. Calculate D for the Δ value at each plate.

$$D = \frac{\Delta R^2 \bar{u}}{x}$$

Plate Number	Δ	D_{ex}
1	2.40×10^{-3}	8.94×10^{-7}
2	4.58×10^{-3}	7.12×10^{-7}
3	7.20×10^{-3}	7.64×10^{-7}
4	1.07×10^{-2}	8.18×10^{-7}

Compare with theoretical D obtained from Equation 8.

Particle Size, μm	$D_{,Th}$
.42	7.8×10^{-7}

Comparison may also be made between the actual particle size and the particle size predicted by the experimental Diffusion coefficient. Figure 17 relates D and particle size.

D_{ex}	Predicted Particle Size, μm
8.94×10^{-7}	.375
7.12×10^{-7}	.445
7.64×10^{-7}	.410
8.18×10^{-7}	.405

The actual particle size was found to be .42 μm using an aerosol centrifuge.

Table 15. Corrected N/N_o and Associated Δ

T = 295°K Experimental Trial	1		2		3		4	
	N/N_o	Δ						
17	.958	2.40×10^{-3}	.935	4.58×10^{-3}	.910	7.2×10^{-3}	.876	1.23×10^{-2}
16 & 10	.969	1.51×10^{-3}	.940	4.0×10^{-3}	.926	9.5×10^{-3}	.905	8.0×10^{-3}
15	.950	3.0×10^{-3}	.913	6.9×10^{-3}	.882	1.1×10^{-2}	.840	1.86×10^{-2}
T = 257°K	1		2		3		4	
	N/N_o	Δ						
16	.958	2.40×10^{-3}	.921	6.0×10^{-3}	.895	9.4×10^{-3}	.860	1.5×10^{-2}
10	.927	5.45×10^{-3}	.870	1.31×10^{-2}	.767	3.55×10^{-2}	.732	4.55×10^{-2}
T = 201° K	1		2		3		4	
	N/N_o	Δ						
10	.938	4.3×10^{-3}	.884	1.09×10^{-2}	.849	1.68×10^{-2}	.803	2.65×10^{-2}
16	.914	6.8×10^{-3}	.837	1.92×10^{-2}	.786	$x.14\times10^{-2}$	.731	4.59×10^{-2}
15	.773	3.4×10^{-2}	.714	5.1×10^{-2}	.641	7.5×10^{-2}	.615	8.35×10^{-2}

Table 16. Comparison of Theoretical and Experimental D

T = 295°K Experimental Trial	Particle Size, μm	D_{Th}	D_{ex} at Each Plate 1	2	3	4
17	.42	7.8×10^{-7}	8.94×10^{-7}	7.12×10^{-7}	7.64×10^{-7}	9.35×10^{-7}
10 & 16	.51	6.1×10^{-7}	5.62×10^{-7}	6.21×10^{-7}	5.84×10^{-7}	6.09×10^{-7}
15	.33	1.07×10^{-7}	1.129×10^{-7}	1.07×10^{-6}	1.17×10^{-6}	1.415×10^{-6}
	Known Particle Size, μm		Predicted Particle Size 1	2	3	4
	.42		.375	.445	.410	.365
	.51		.54	.51	.52	.51
	.33		.31	.325	.30	.265

T = 275°K Experimental Trial	Particle Size, μm	D_{Th}	D_{ex}			
16	.51	5.60×10^{-7}	7.78×10^{-7}	8.12×10^{-7}	8.7×10^{-7}	9.42×10^{-7}
10	.375	8.20×10^{-7}	1.765×10^{-6}	1.77×10^{-6}	3.28×10^{-6}	3.01×10^{-7}
	Known Particle Size, μm		Predicted Particle Size			
	.51		.39	.375	.355	.325
	.375		.23	.225	.144	.15

Table 16. (Continued)

T = 201°K

Experimental Trial	Particle Size, μm	D_{Th}	D_{ex} 1	2	3	4
10	.51	4.90×10^{-7}	1.113×10^{-6}	1.179×10^{-6}	1.239×10^{-6}	1.405×10^{-6}
16	.40	6.60×10^{-7}	1.76×10^{-6}	2.075×10^{-6}	2.32×10^{-6}	2.425×10^{-6}
15	.30	9.60×10^{-7}	8.8×10^{-6}	5.52×10^{-6}	5.55×10^{-6}	4.42×10^{-6}

Known Particle Size, μm	Predicted Particle Size 1	2	3	4
.51	.267	.258	.248	.225
.40	.190	.170	.156	.150
.30	.067	.090	.089	1.01

APPENDIX E

EXPERIMENTAL DATA, FIRST ARRANGEMENT

Table 17. Concentration Data-I

CHS	Time, sec	Concentration $\mu gm/m^3$
Zero	175	411
	575	409
	975	427
	1475	437
	1875	439
	2275	453
	2675	474
1	375	404
	2075	444
2	775	404
	2475	454
3	1275	349
4	1675	229

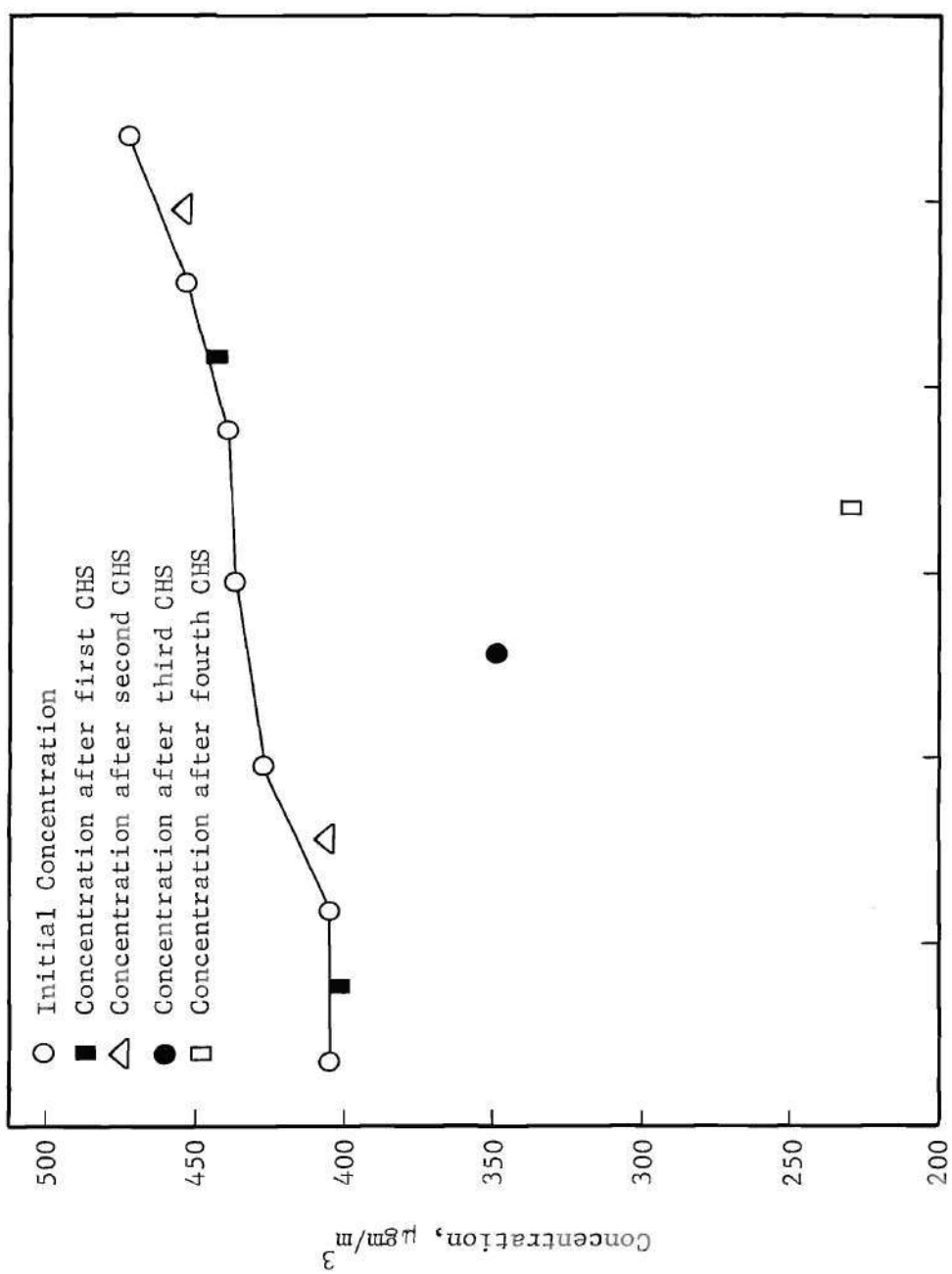

Figure 18. Concentration Data I

Table 18. Concentration Data-II

CHS	Time, sec	Concentration $\mu gm/m^3$
Zero	875	291
	1275	274
	1675	252
	2075	224
	2475	234
	2775	216
	3175	205
	3575	198
1	1075	283
	2975	217
2	1475	264
	3375	206
3	1875	218
4	2275	195

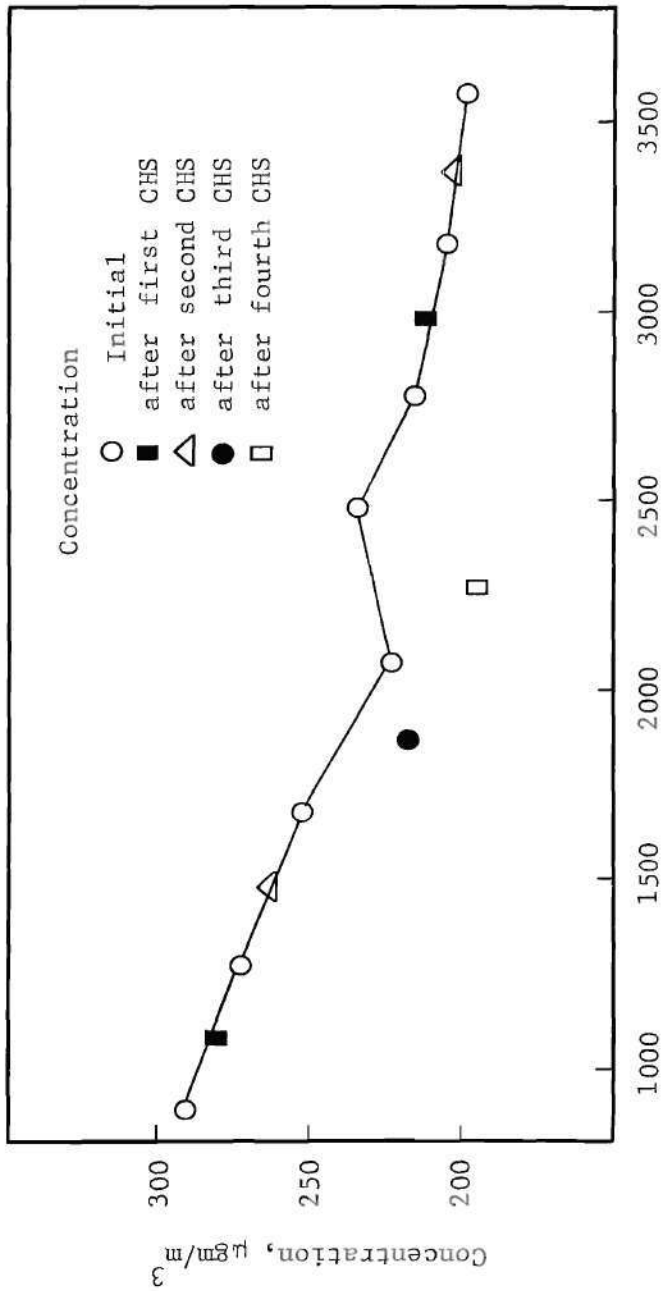

Figure 19. Concentration Data II

Table 19. Concentration Data-III

CHS	Time, sec	Concentration $\mu gm/m^3$	CHS	Time, sec	Concentration $\mu gm/m^3$
Zero	2175	442	3	2975	381
	2375	444		3575	385
	2575	444		4175	410
	3075	413		4775	350
	3375	426		5775	392
	3675	431			
	3975	430	4	1975	357
	4275	465		2775	327
	4575	469		3275	330
	4875	433		3875	303
	5175	418		4475	312
	5475	443		5075	307
	5675	439		5975	359
	5875	469			
	6075	467			
	6275	506			

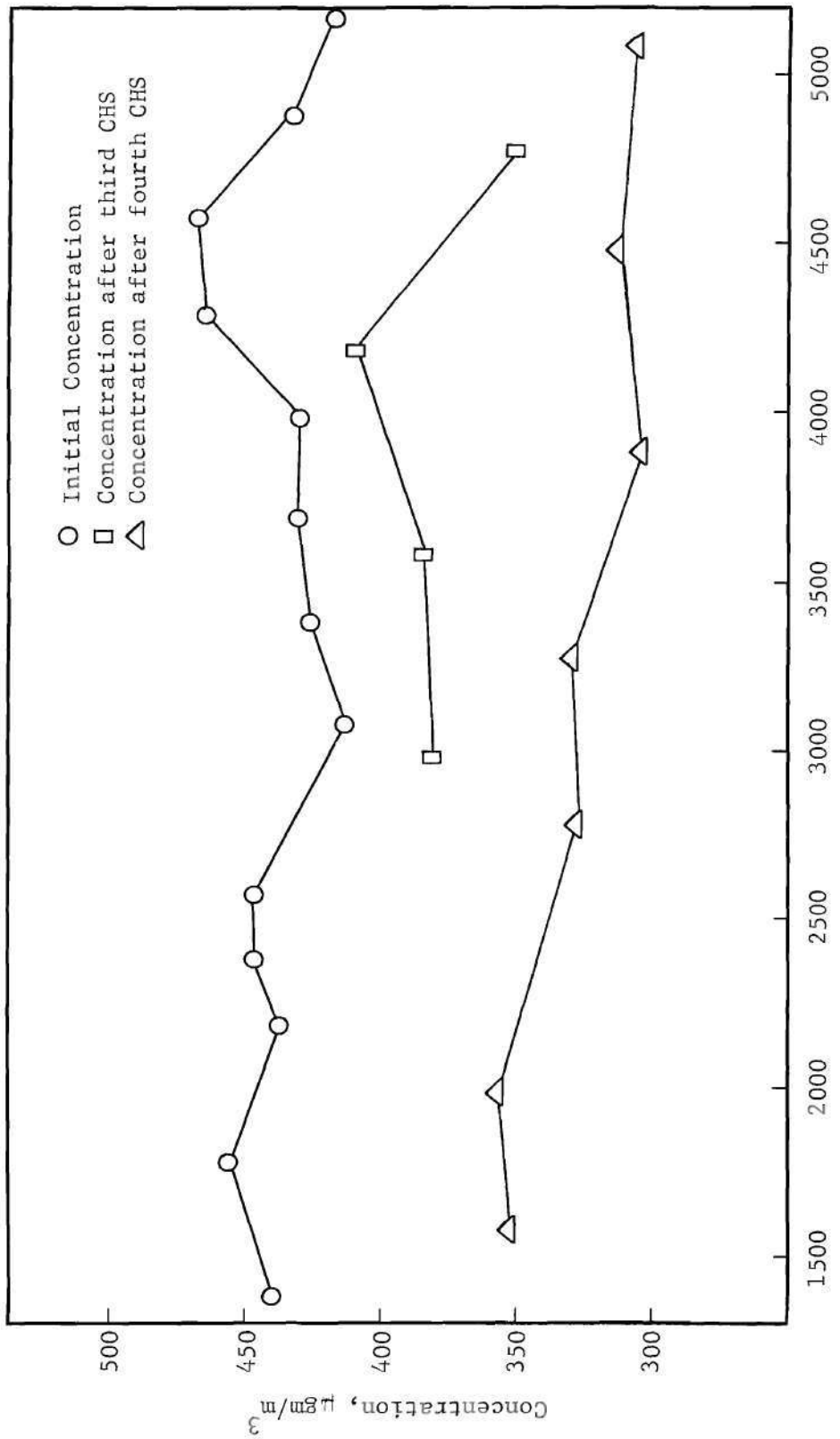

Figure 20. Concentration Data III

Table 20. Concentration Data-IV

CHS	Time, sec	Concentration μ gm/m^3
Zero	2425	406
	2725	412
	3025	405
	3325	405
	4825	409
	6025	407
3	3175	390
	3775	379
	4675	382
	5275	374
4	2575	340
	2875	330
	3475	338
	4375	334
	4975	343
	5575	333

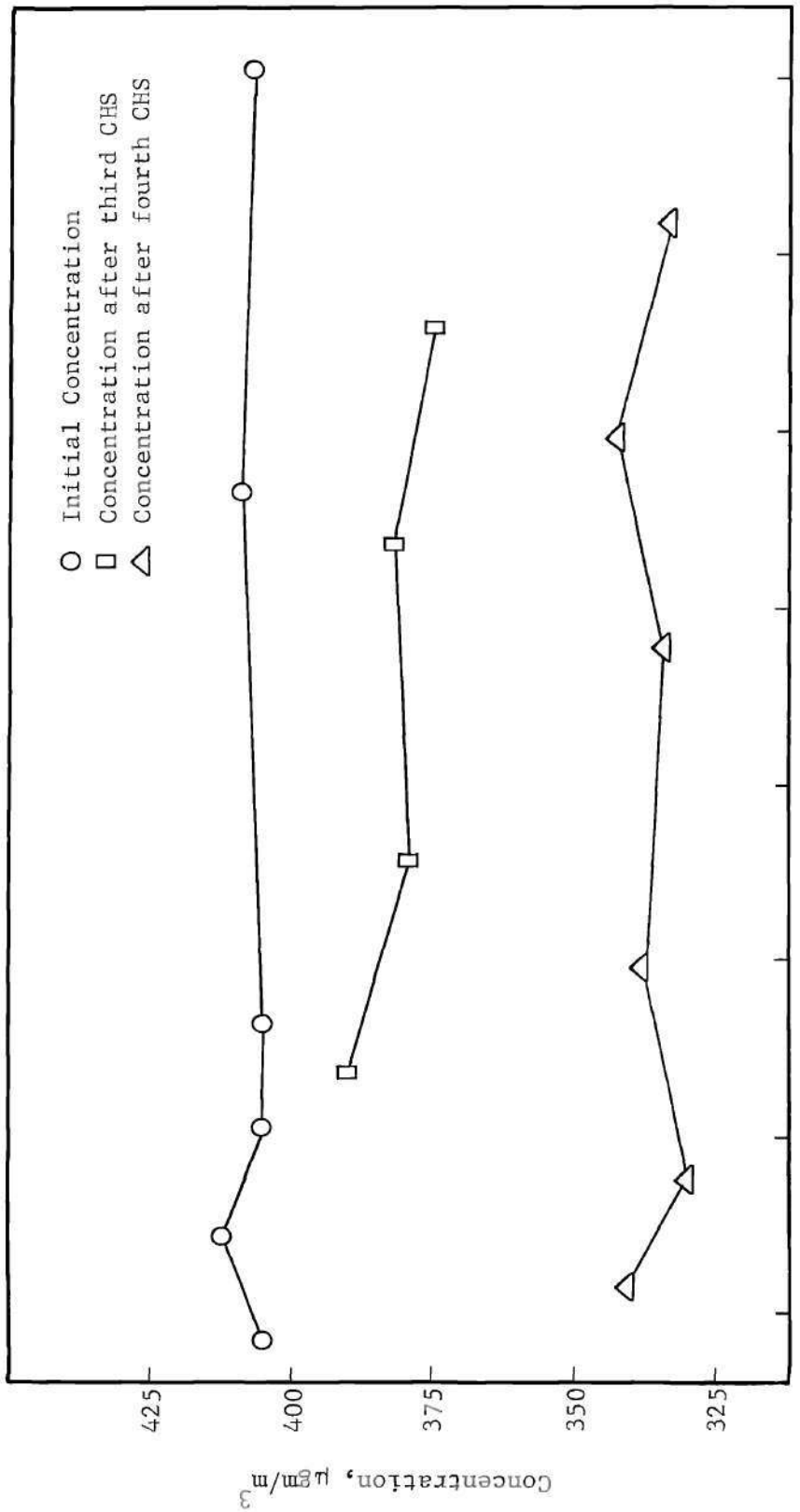

Figure 21. Concentration Data IV

Table 21. Concentration Data-V

CHS	Time, sec	Concentration $\mu gm/m^3$	CHS	Time, sec	Concentration $\mu gm/m^3$
Zero	475	325	3	1125	289
	675	339		1575	333
	775	340		2025	335
	1275	358		2475	328
	1725	383		3075	276
	2175	395			
	2625	375	4	975	244
	2925	352		1425	270
	3225	340		1875	291
				2325	305
				2775	254

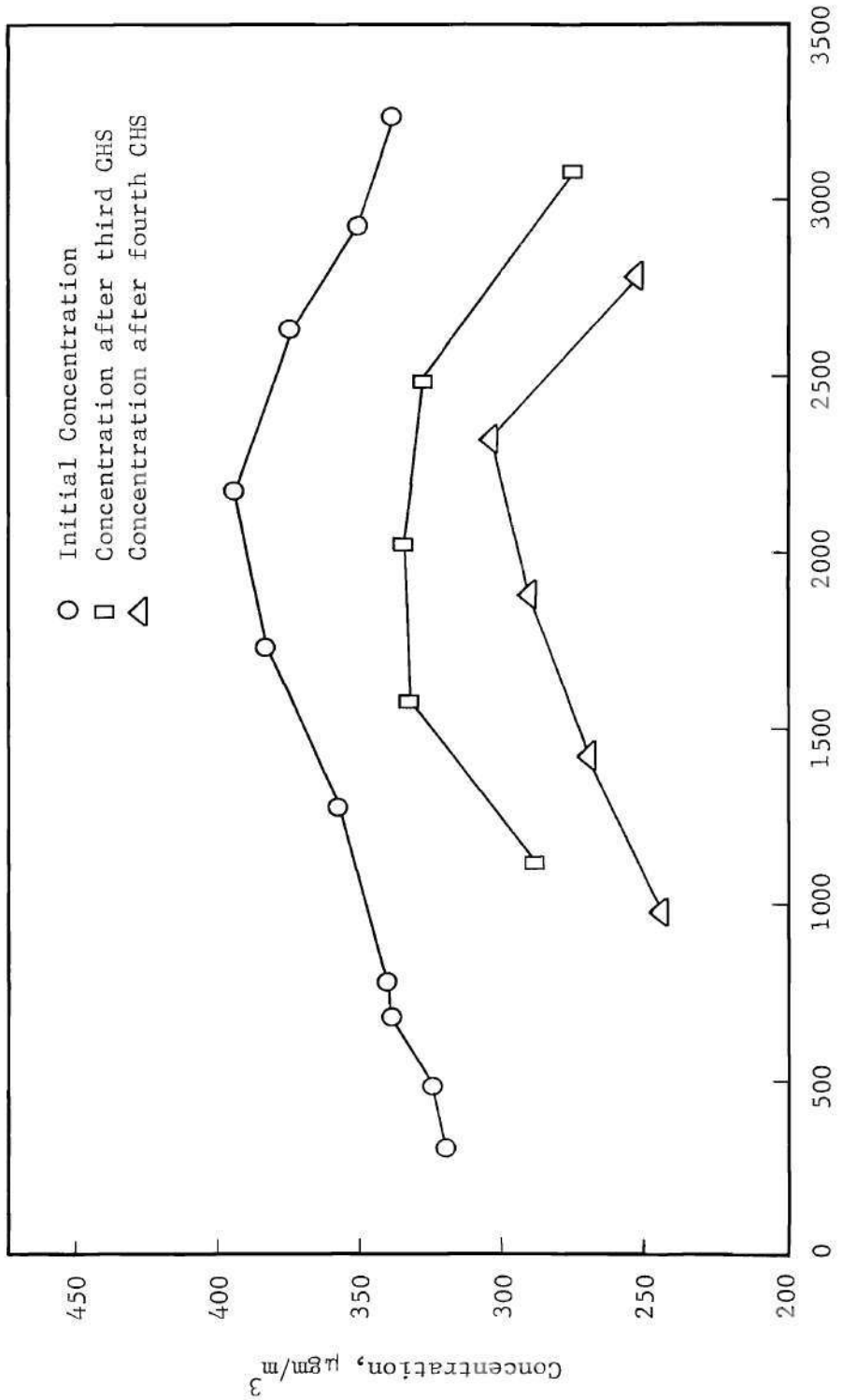

Figure 22. Concentration Data V

Table 22. Concentration Data VI

CHS	Time, sec	Concentration $\mu gm/m^3$
Zero	1800	298
	2400	292
	2800	292
	3200	320
	3600	335
	4000	352
	4400	375
	4800	402
	5200	434
	5600	480
	6000	524
3	1600	271
	2600	250
	3400	292
	4200	319
	5000	375
	5800	453
4	1200	247
	2200	222
	3000	229
	3800	271

Table 22. (Continued)

CHS	Time, sec	Concentration $\mu gm/m^3$
	4600	297
	5400	362

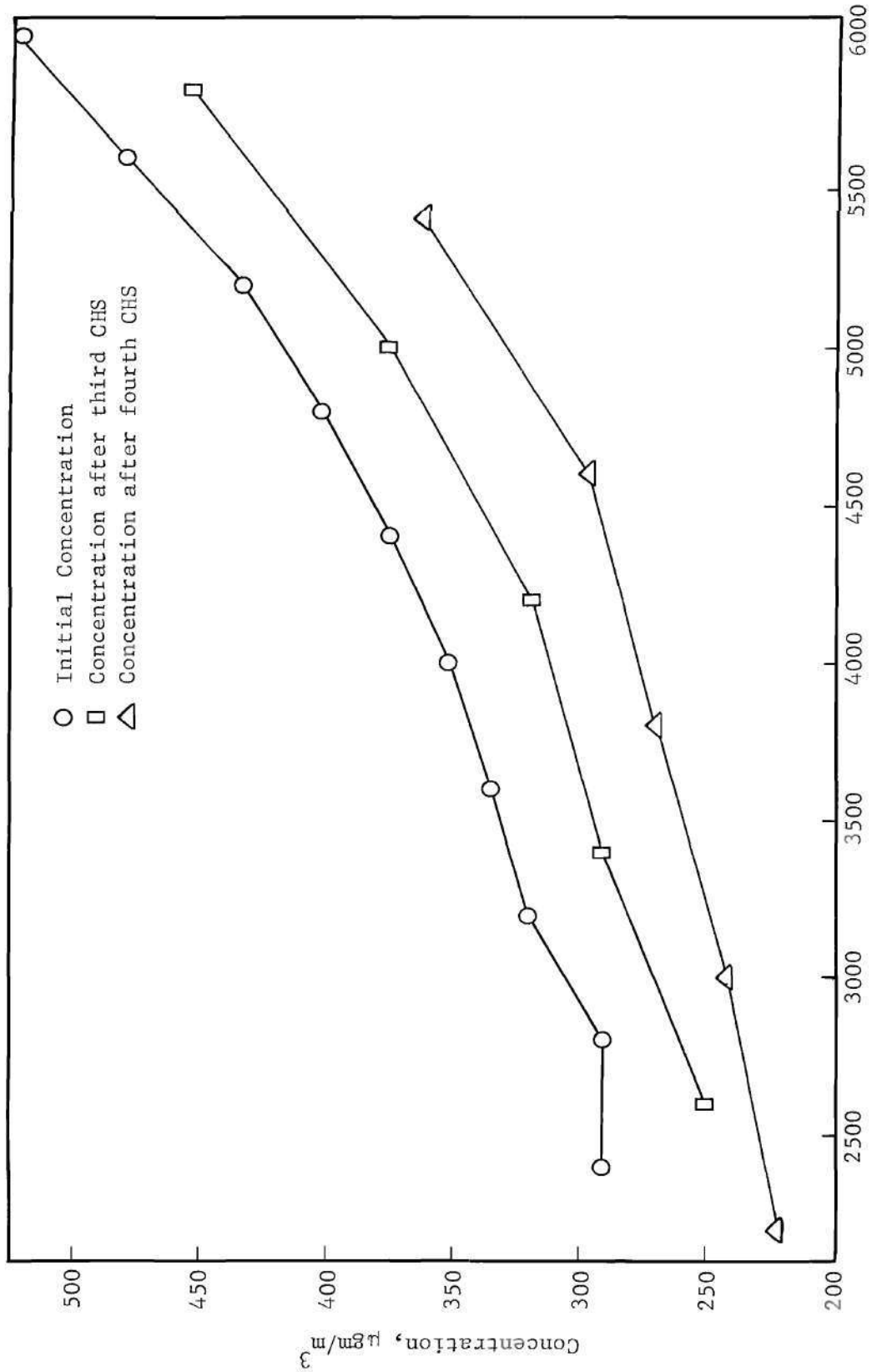

Figure 23. Concentration Data VI

Table 23. Concentration Data VII

CHS	Time, sec	Concentration $\mu gm/m^3$
Zero	1900	226
	2300	227
	2700	228
	3100	224
	3500	227
	3900	229
	4300	238
	4700	242
	5100	271
3	2100	200
	2900	192
	4100	204
	4500	215
4	2500	175
	3300	174
	3700	175
	4900	204

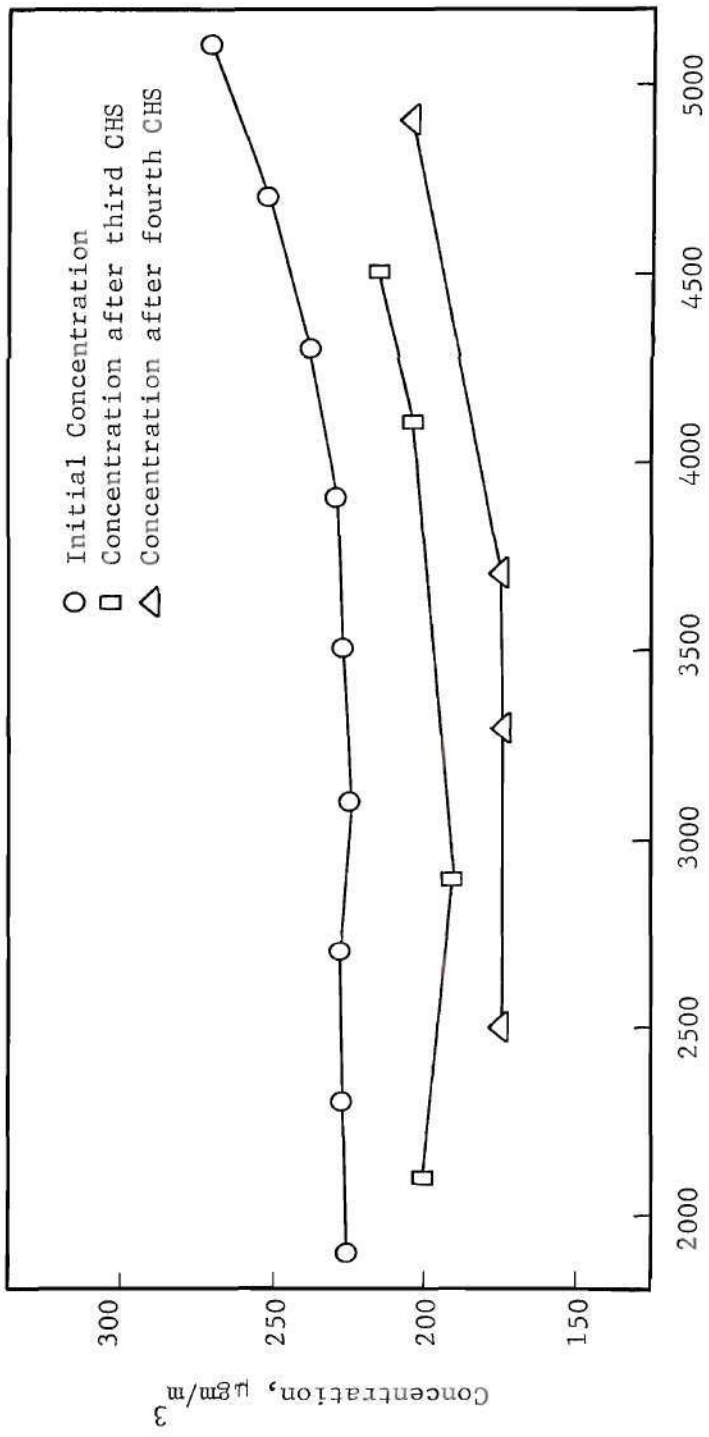

Figure 24. Concentration Data VII

APPENDIX F

EXPERIMENTAL DATA, SECOND ARRANGEMENT

Table 24. Concentration Data from Test 10 at 22 C

CHS	Time, sec	Concentration $\mu gm/m^3$	CHS	Time, sec	Concentration $\mu gm/m^3$
Zero	1000	264	1	1200	239
	1400	265		2800	229
	1800	253.5		4400	231
	2200	242		6000	218
	2600	254		7800	220
	3000	228			
	3400	231			
	3800	240	2	1600	227
	4200	237		4800	198
	4600	237		4800	198
	5000	227		6400	200
	5400	238		8200	207
	5800	234			
	6200	229			
	6600	235	3	2400	207
	7000	225		3600	199
	7400	238		5200	179
	7600	233		6800	171
	8000	235.5		8600	184

Table 24. (Continued)

CHS	Time, sec	Concentration $\mu gm/m^3$	CHS	Time, sec	Concentration $\mu gm/m^3$
	8400	230			
	8800	237			
	9200	241	4	2000	182.5
				4000	179
				5600	169
				7200	162
				9000	175

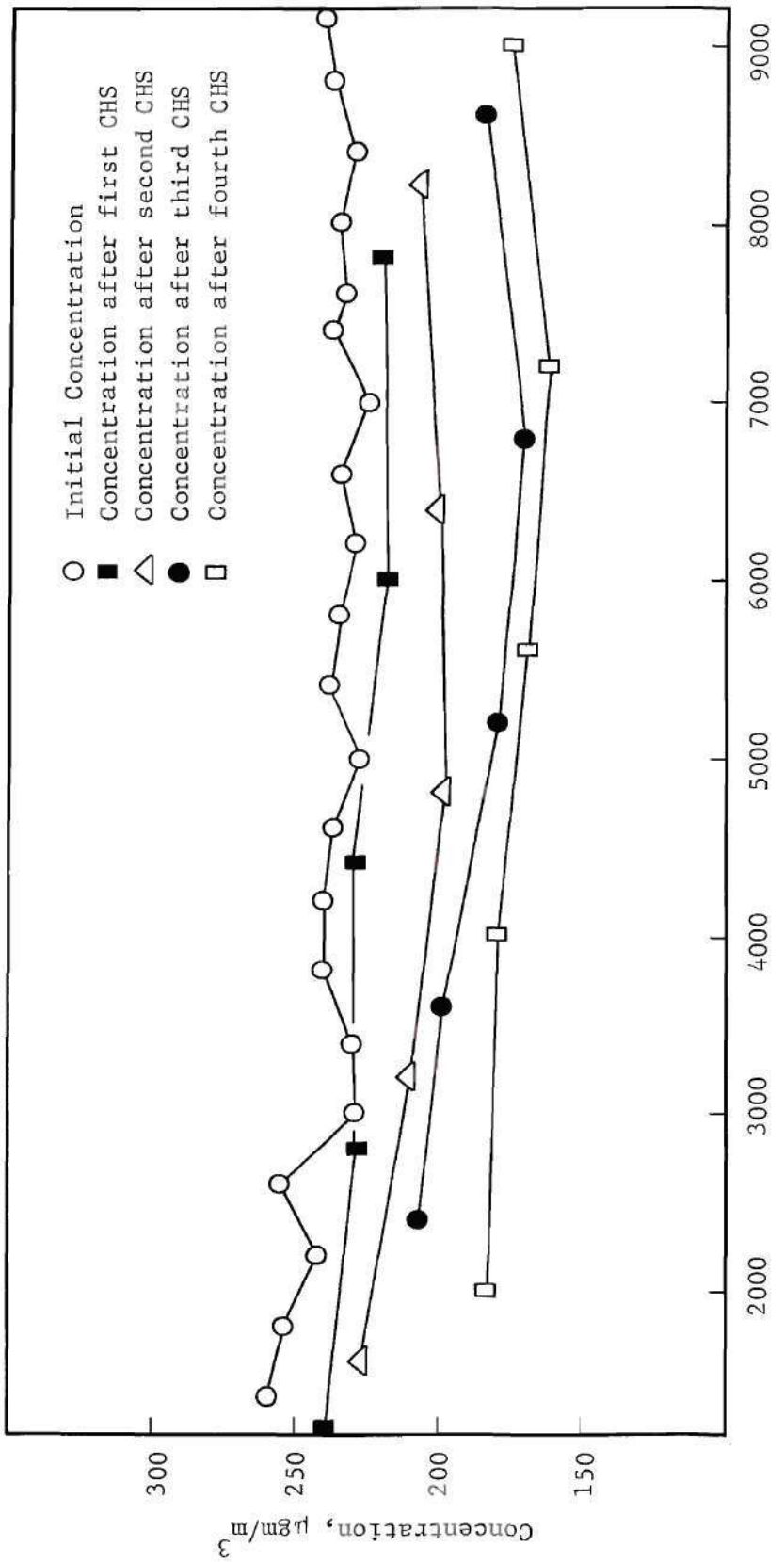

Figure 25. Concentration Data from Test 10 at 22 °C

Table 25. Concentration Data from Test 15 at 22 C

CHS	Time, sec	Concentration $\mu gm/m^3$	CHS	Time, sec	Concentration $\mu gm/m^3$
Zero	1600	216.5	1	1800	212.5
	2000	214.5		3400	234
	2400	255		5000	285
	2800	273		6600	332
	3200	244			
	3600	279			
	4000	282	2	2200	212
	4400	287.5		3800	237
	4800	307		5400	264
	5200	315			
	5600	313.5			
	6000	329	3	2600	197.5
	6400	347		4200	208
	6800	351		5800	255
			4	3000	169
				4600	169
				4600	202.5
				6200	229

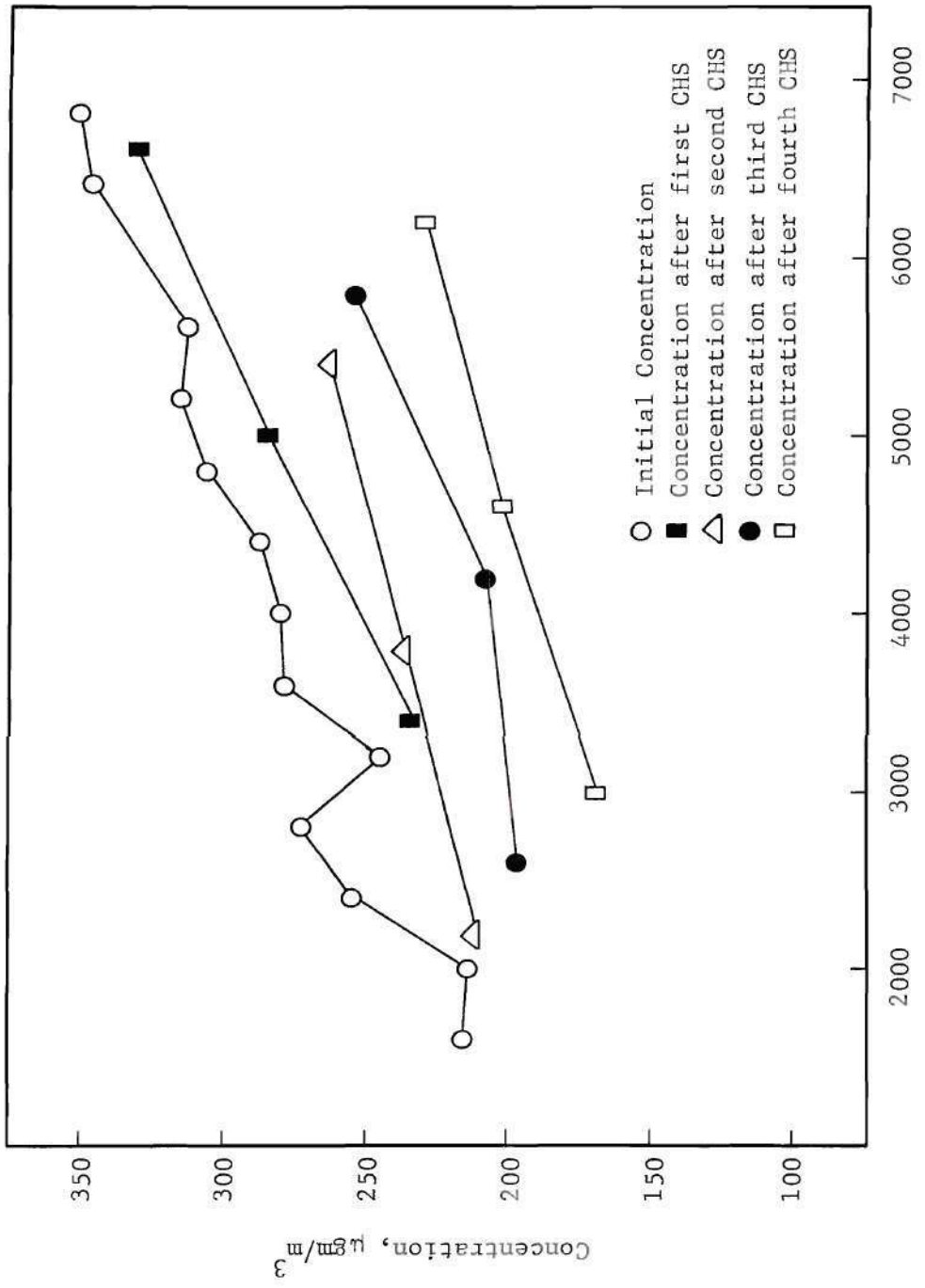

Figure 26. Concentration Data from Test 15 at 22 °C

Table 26. Concentration Data from Test 16 at 22 C

CHS	Time, sec	Concentration $\mu gm/m^3$	CHS	Time, sec	Concentration $\mu gm/m^3$
Zero	300	359	1	700	336.5
	500	355		2300	363
	900	358		3900	371
	1300	375		5500	374
	1700	376			
	2100	382			
	2500	380	2	1100	331
	2900	383		2700	338
	3300	377		4300	364
	3700	393		5900	359
	4100	402			
	4500	423			
	4900	412	3	1500	304
	5300	408		3100	309
	5700	415		4700	344
	6100	424		6300	332
	6500	419			
	6900	420			
			4	1900	270
				3500	273
				5100	289
				6700	289

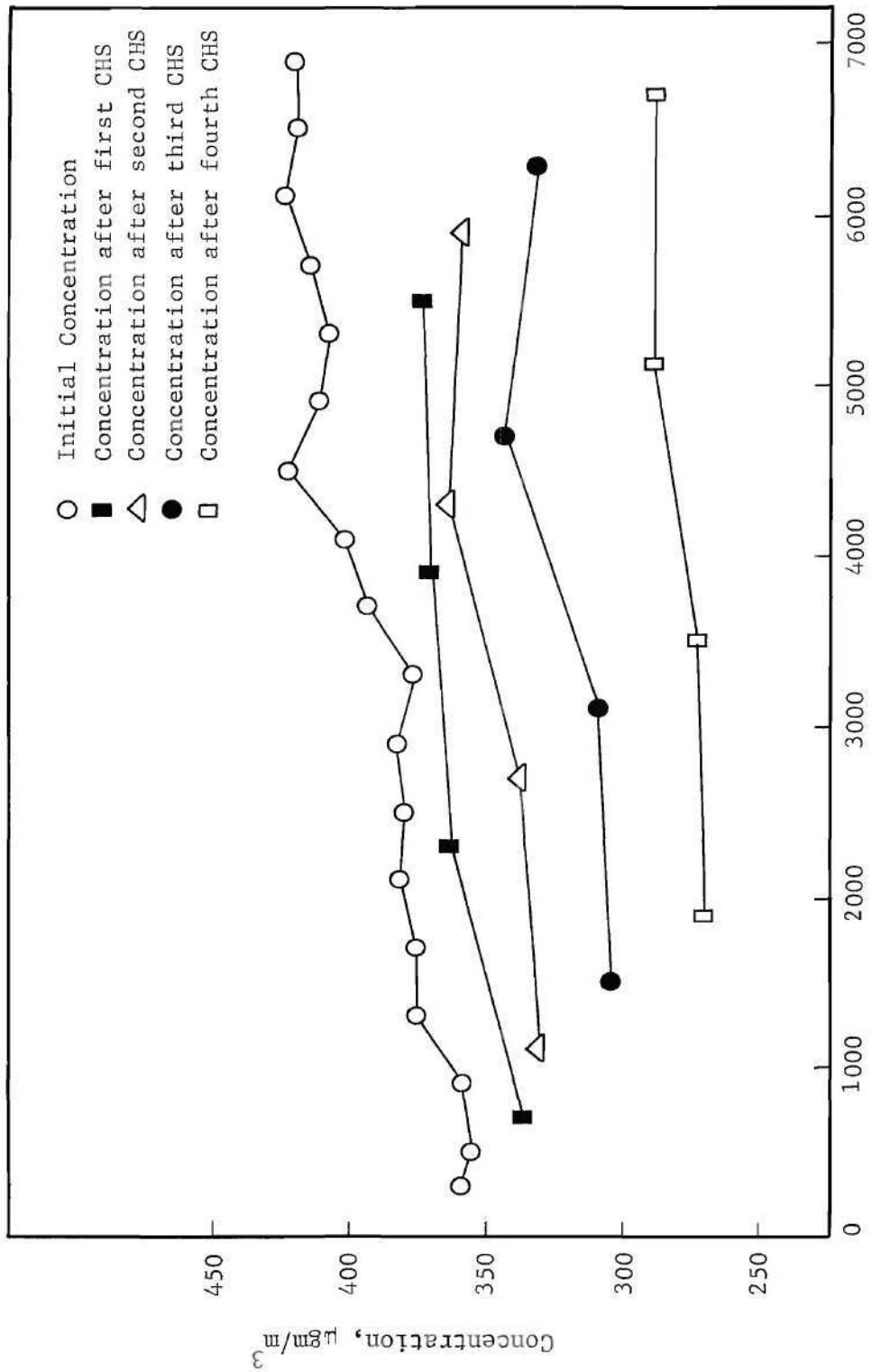

Figure 27. Concentration Data from Test 16 at 22 °C

Table 27. Concentration Data from Test 17 at 22 C

CHS	Time, sec	Concentration $\mu gm/m^3$	CHS	Time, sec	Concentration $\mu gm/m^3$
Zero	700	250	1	900	227
	1100	251.5		4100	225
	1500	240		4500	225
	1900	239.5		7300	225
	2300	238.5		7700	239
	3100	236.5			
	3500	236.5	2	1300	215
	3900	236.5		3700	201
	4300	245		4900	213.5
	4700	246.2		6900	206
	5700	245		8100	215
	5500	242.5			
	5900	241.5			
	6300	243	3	1700	202
	6700	238		2400	179.5
	7100	243		3300	179
	7500	248		5300	192
	7900	250		6500	173.5
	8300	252.5	8500	233	
	8700	289			
	9100	293			

Table 27. (Continued)

CHS	Time, sec	Concentration $\mu gm/m^3$	CHS	Time, sec	Concentration $\mu gm/m^3$
			4	2100	163.5
				2500	165.5
				5700	177
				6100	175
				8900	236.5

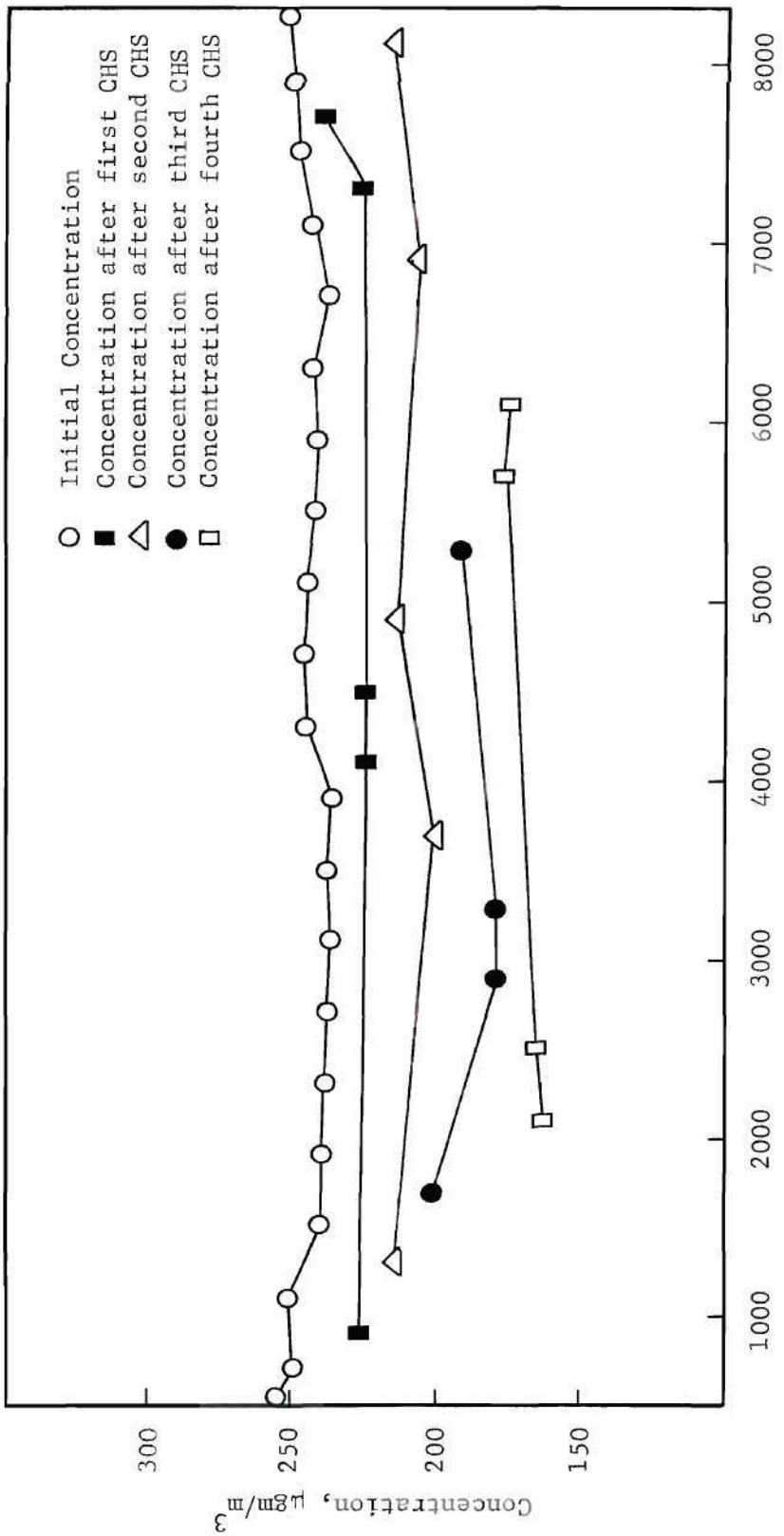

Figure 28. Concentration Data from Test 17 at 22 °C

Table 28. Concentration Data from Test 10 at -16 C

CHS	Time, sec	Concentration $\mu gm/m^3$	CHS	Time, sec	Concentration $\mu gm/m^3$
Zero	300	208.5	1	2500	179
	500	213.5		4100	197
	700	212		5500	204
	900	206		7100	175
	1300	211			
	1900	198			
	2300	203	2	2100	161
	2700	203		3700	158
	3100	205		5100	177
	3500	204		6700	157.5
	3900	212			
	4900	221.5			
	5300	218	3	1500	138
	6100	211		3300	133
	6500	201		6300	139
	6900	198			
	7300	195.5			
	7700	192	4	1100	114
				2900	114
				4300	129.5
				5900	127.5
				7500	109.5

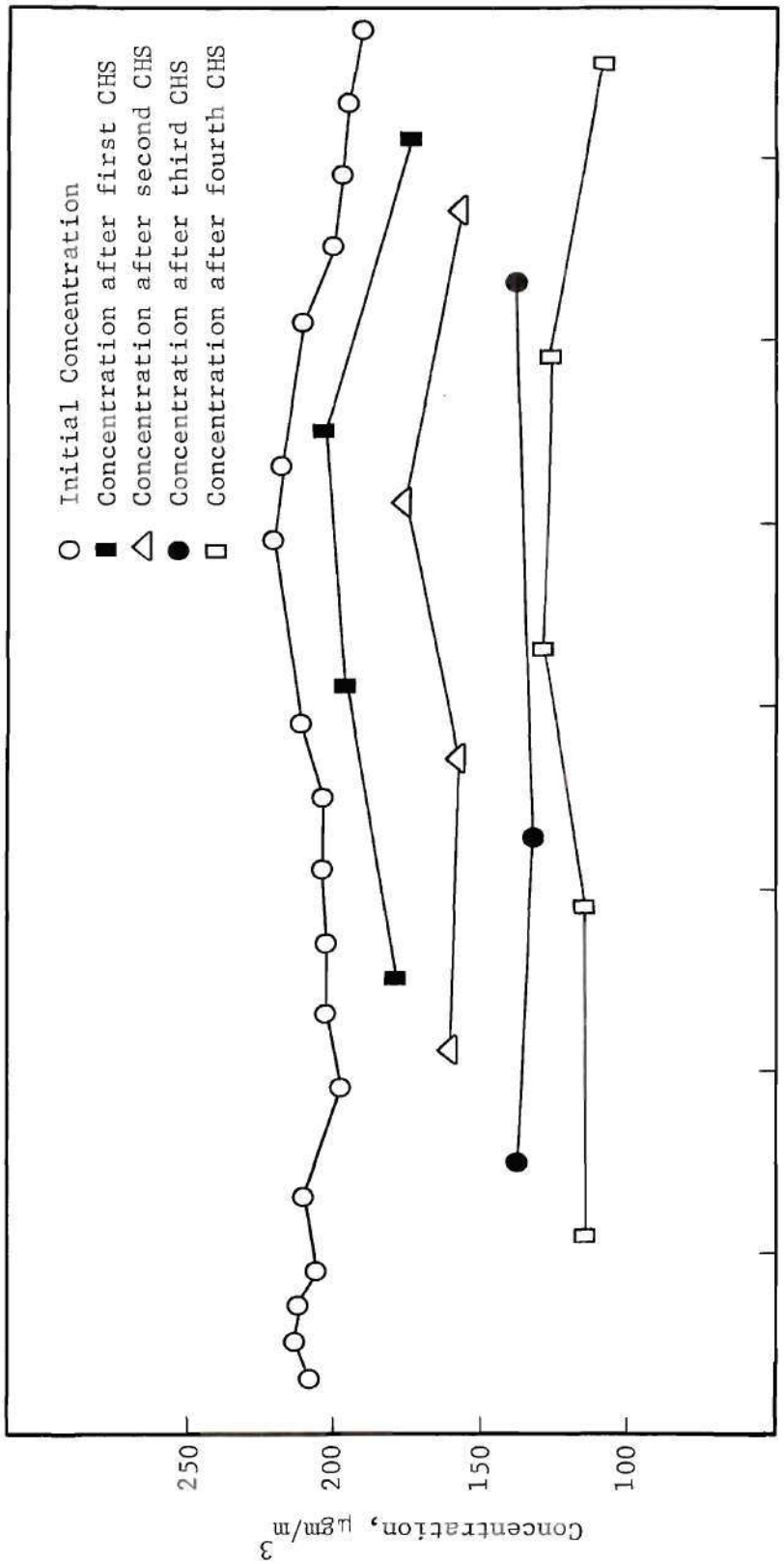

Figure 29. Concentration Data from Test 10 at -16 °C

Table 29. Concentration Data from Run 16 at -16 C

CHS	Time, sec	Concentration $\mu gm/m^3$	CHS	Time, sec	Concentration $\mu gm/m^3$
Zero	300	358	1	900	351
	500	346		2500	368
	700	351		4100	350
	1100	388	5750	370	
	1500	399			
	1900	397			
	2300	401	2	1300	338
	2700	384		2900	331
	3500	371		4450	326
	3900	362		6150	339
	4650	380			
	5050	379			
	5550	398	3	1700	321
	5950	401		3300	299
	6350	398		4850	301
	6750	414		6550	315
	7150	408			
			4	2100	280
				3700	273
				5350	253
				6950	282

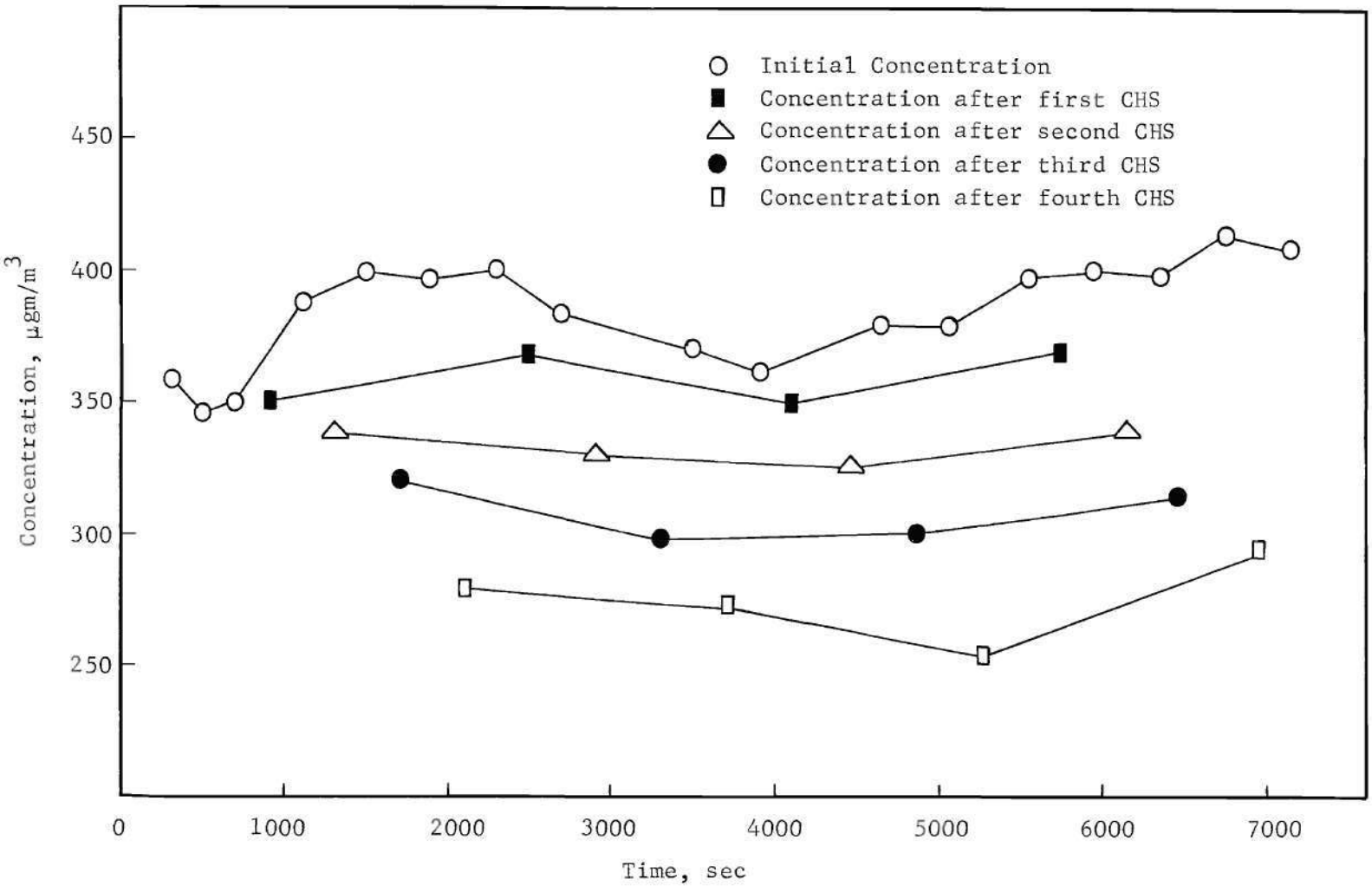

Figure 30. Concentration Data from 16 at -16 °C

Table 30. Concentration Data from Test 10 at -72 C

CHS	Time, sec	Concentration $\mu gm/m^3$	CHS	Time, sec	Concentration $\mu gm/m^3$
Zero	1000	191	1	2600	154
	1200	175		4200	142
	1600	174		5800	139
	2000	170		7400	130.5
	2400	173	9000	109	
	2800	174			
	3200	165.5			
	3600	145	2	2200	133.5
	4000	154		3800	129
	4400	145	5400	128.5	
	4800	146.5		7000	125.5
	5200	151.5		8600	94.5
	5600	152.5			
	6000	163			
	6400	147	3	1800	122.5
	6800	150		3400	118.2
	7200	149		5000	112
	7600	138.5		6600	115
	8000	134.5		8200	92
	8400	130.5			
	8800	121.5			

Table 30. (Continued)

CHS	Time, sec	Concentration $\mu gm/m^3$	CHS	Time, sec	Concentration $\mu gm/m^3$
	9200	130.5	4	1400	115.5
				3000	109.1
				4600	98.4
				6200	106.5
				7800	83

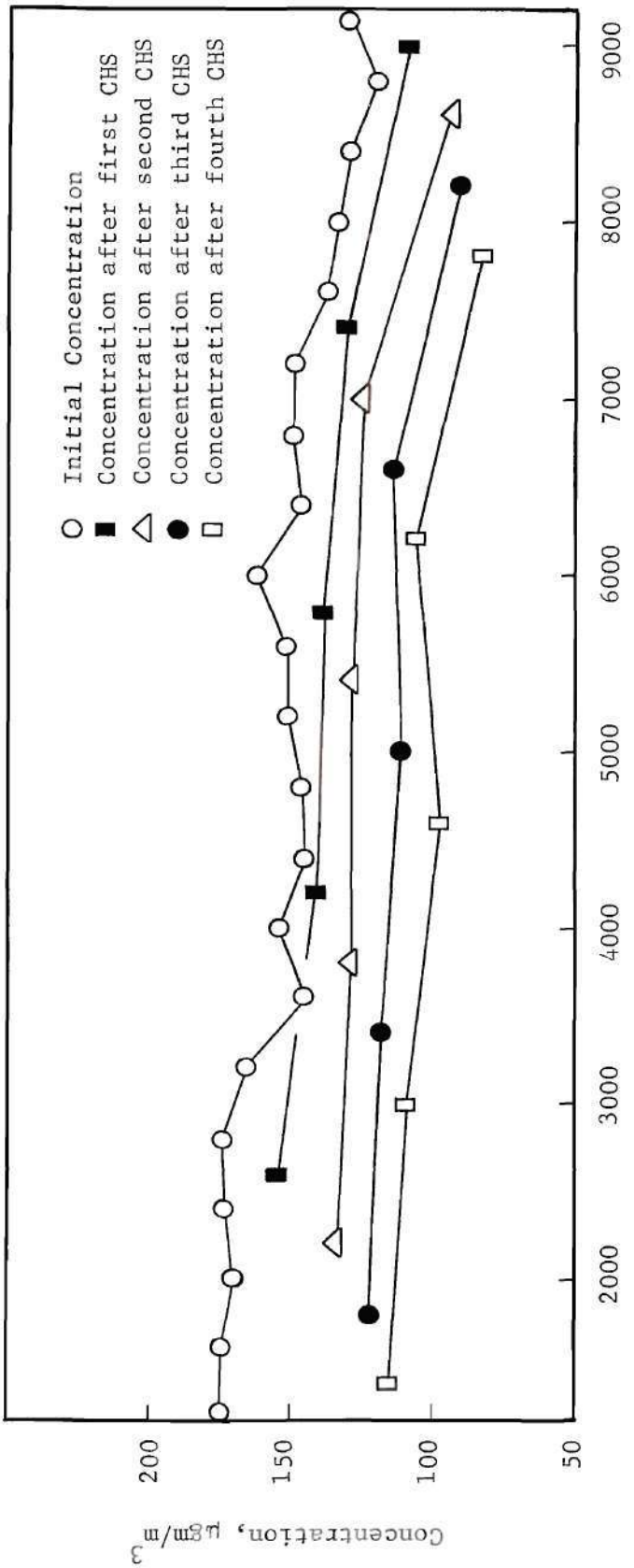

Figure 31. Concentration Data from Test 10 at -72 °C

Table 31. Concentration Data from Test 15 at -72 C

CHS	Time, sec	Concentration $\mu gm/m^3$	CHS	Time, sec	Concentration $\mu gm/m^3$
Zero	1400	268.5	1	1600	235
	1800	275		3200	186
	2200	270		4800	173
	2600	262		7600	170
	3000	252		8000	178
	3400	244			
	3800	249			
	4200	244	2	2000	191.5
	4600	235		3600	152.5
	5000	233.5		5200	146.4
	5400	234.5		7200	148.5
	5800	237		8400	148
	6200	222.5			
	6600	234.5			
	7000	225	3	2400	165
	7400	226.5		4000	141.5
	7800	226		5600	132
	8200	218.5		6800	128.5
	8600	211.5		8800	134.5
	9000	212			
	9400	203			

Table 31. (Continued)

CHS	Time, sec	Concentration $\mu gm/m^3$	CHS	Time, sec	Concentration $\mu gm/m^3$
			4	2800	129.5
				4400	121
				6000	112.5
				6400	117
				9200	115.1

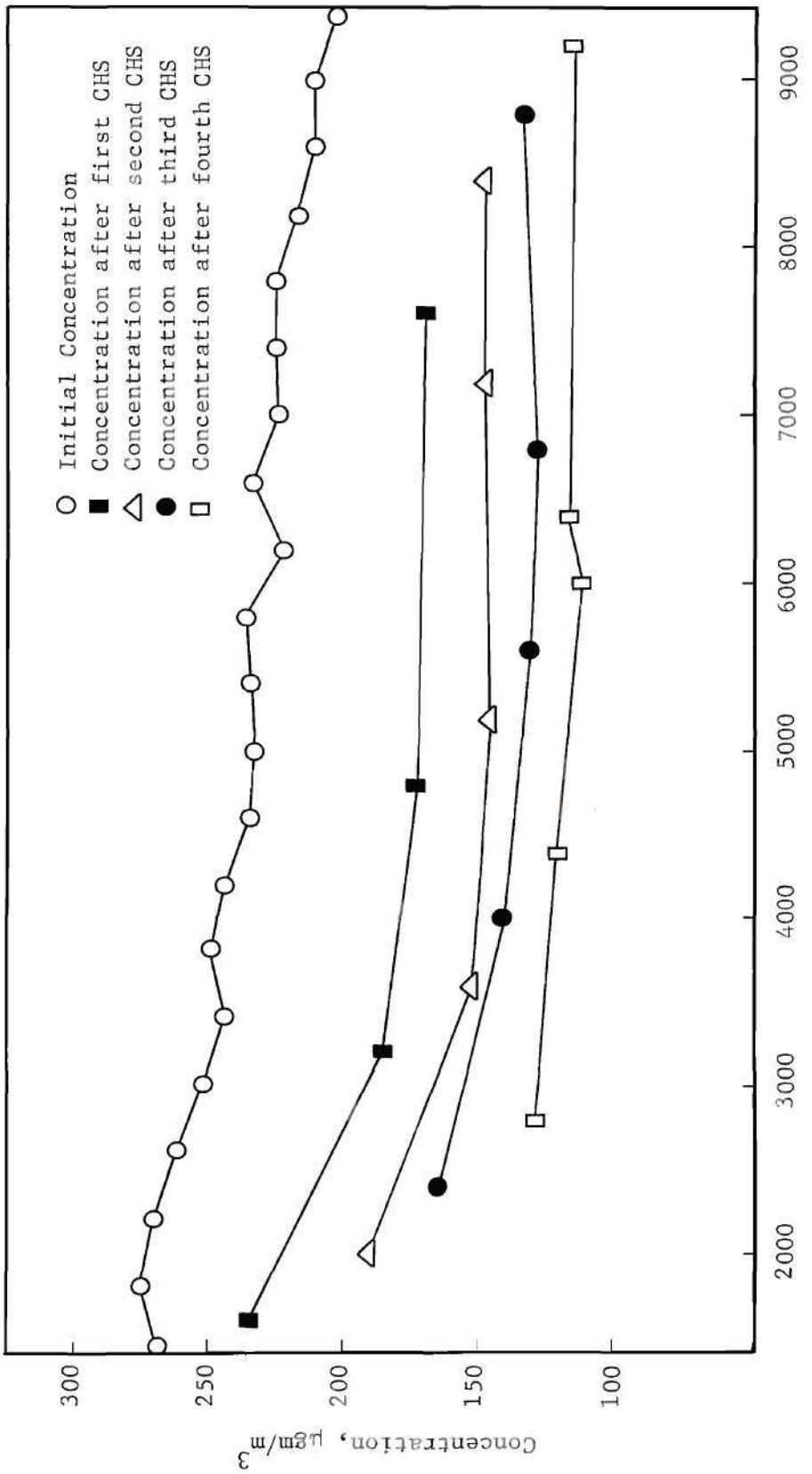

Figure 32. Concentration Data from Test 15 at -72 °C

Table 32. Concentration Data from Test 16 at -72 C

CHS	Time, sec	Concentration $\mu gm/m^3$	CHS	Time, sec	Concentration $\mu gm/m^3$
Zero	1100	349	1	1300	305
	1500	340		2900	302
	1900	351		4500	254
	2300	339		6100	172.5
	2700	334			
	3100	325			
	3500	318	2	1700	251
	2900	296		3300	235
	4300	296		4900	211
	4700	280		6500	115.5
	5100	264			
	5500	250			
	5900	243	3	2100	225
	6300	163		3700	205
	6700	131		5300	179.5
			4	2500	198
				4100	181
				5700	146.5

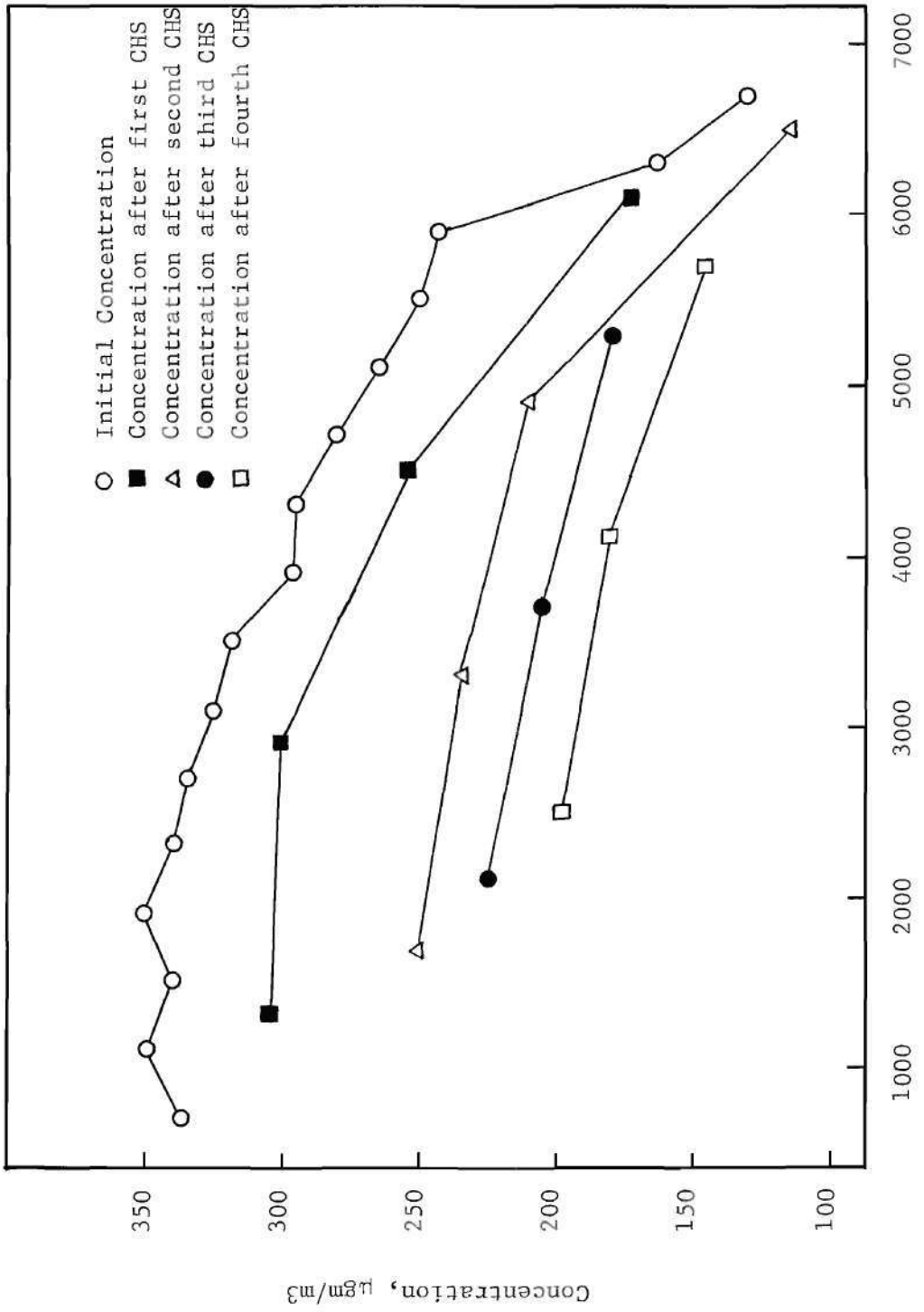

Figure 33. Concentration Data from Test 16 at -72 °C

BIBLIOGRAPHY

1. Thomas, J. W., J. Colloid Interface Sci., 10, 246-255 (1955).

2. DeMarcus, W., and Thomas, J. W., U.S. Atom. Commiss., ORNL-1413 (1952).

3. Nolan, J. J. and Guerrin, V. H., Proc. Roy. Irish Acad., 43A, 5 (1935).

4. Townsend, J. S., Trans. Roy. Soc. (London) 193A, 129 (1900).

5. Gormley, P. G. and Kennedy, M., Proc. Roy. Irish Acad., 52A, 163-9 (1949).

6. Breslin, A. J., Guggenheim, S. F. and George, A. C., Staub, 31, 8, 313-316 (1971).

7. Einstein, A., Ann. Physik, 17, 549 (1905).

8. Fuchs, N. A., The Mechanics of Aerosols, Pergamon Press, Oxford (1964).

9. Fox, J. J., Matteson, M. J., Preining, O., Nature, 82, 238 (1972).

10. Particle Mass Monitor Instruction Manuel for Thermo-Systems Models 3205A , Thermo-Systems, Inc., St. Paul, Minnesota.

11. Boscoe, G. F., The Calibration of an Aerosol Centrifuge and a Study of Density Deviation in Condensation Aerosols, M. S. Thesis, Georgia Institute of Technology, 1972.

12. Hochrainer, O., J. Colloid Interface Sci., 36, 191-94 (1971).

13. Spurny, K., Lodge, J. P., Frank, E. R., and Sheesley, D. C., Environ. Sci. and Tech., 3 453-464 (1969).